Biology Methods and Protocols, 2026, **11**(1), bpag011
https://doi.org/10.1093/biomethods/bpag011
Published: 15 March 2026
Methods Article

BIOLOGY Methods & Protocols
OXFORD

Enhancing propagation and purification efficiency of M13 bacteriophage for improved phage display applications

Md Monir Hossain[1,2], Foong Yong[2], Vipul Bansal[1,2] and Ravi Shukla[1,2,3,*]

[1]Sir Ian Potter NanoBiosensing Facility, Nanobiotechnology Research Laboratory (NBRL), RMIT University, Melbourne, VIC 3000, Australia
[2]School of Science, RMIT University, Melbourne, VIC 3000, Australia
[3]Centre for Advanced Materials & Industrial Chemistry, RMIT University, Melbourne, VIC 3000, Australia

*Corresponding author. School of Science, RMIT University, 124 La Trobe St, Melbourne VIC 3000, Australia. Email: ravi.shukla@rmit.edu.au

Abstract

The global biosensors market is rapidly growing, driven by increasing demand for quick, affordable, and portable diagnostic tools across sectors, including healthcare, environmental monitoring, food safety, and biomedical research. The key to biosensor function is the biological recognition element (BRE), which determines the specificity, sensitivity, and reliability of the device. Traditional BREs, such as antibodies and enzymes, face significant limitations, including instability, high costs, and variability. Phage display technology offers a strong alternative, providing durable, stable, and highly specific peptides as BREs. However, it requires effective amplification and purification methods to produce high-quality peptide libraries. This study examines key factors affecting the amplification of filamentous M13 bacteriophage, highlighting the negative impact of high multiplicity of infection (MOI) caused by superinfection exclusion and reduced phage adsorption efficiency. Our findings indicate that the bacterial growth phase is the most important determinant of M13 amplification efficiency. Furthermore, post-infection PEG/NaCl precipitation followed by high-speed centrifugation significantly outperforms traditional filtration methods in purifying phages, maximizing recovery and viability. These findings present an optimized, reproducible, and scalable approach to M13 phage amplification, improving the effectiveness of phage display for developing advanced biorecognition elements. Ultimately, this research provides a foundational framework for more efficient biosensing and therapeutic applications, filling critical gaps in the current biosensor development landscape.

Keywords biosensors, phage display, M13 bacteriophage, biorecognition elements (BREs), peptide libraries, multiplicity of infection (MOI), superinfection exclusion, diagnostics

Introduction

The global biosensors market, valued at USD 32.14 billion in 2024, is projected to reach USD 75.84 billion by 2033, growing at a CAGR of 10.40% during the forecast period of 2025–2033, indicating strong demand for fast, affordable, and portable testing devices [1]. Currently, over 70% of clinical decisions depend on diagnostic tests, and biosensors are playing an increasingly important role [2, 3]. Beyond healthcare, they are also used in environmental monitoring, food safety, drug research, forensic science, and biomedical research [4–7].

A biosensor detects specific biological substances and converts that detection into a measurable signal. It comprises three main parts: a biological recognition element (BRE), a transducer, and a signal processor [4, 8]. The BRE is the primary component of the biosensor and is responsible for binding to the target substances, known as analytes. These biological recognition elements (BREs) include enzymes, antibodies, peptides, or aptamers, each chosen for their ability to interact with specific targets like glucose, toxins, or viruses [8, 9]. Once the BRE captures the target, the transducer converts this interaction into a physical signal, such as changes in electric current, light, heat, or pH [8, 10]. This signal is then sent to the signal processor, which amplifies it and displays the result in a user-friendly format, such as a number on a screen or a colour change [9]. These systems are remarkably impactful in medical diagnostics due to their rapid response, specificity, and potential for point-of-care use [8].

Despite advances in biosensor technology, creating effective and reliable BREs remains a significant challenge. Traditional probes, such as antibodies and enzymes, are widely used but have limitations [11]. Antibodies, although highly specific, are costly to produce, sensitive to environmental factors like pH and temperature, and can vary

Received: 19 November 2025; **Revised:** 10 February 2026; **Accepted:** 11 February 2026

between batches. Besides, antibodies cannot be produced against every target/analyte that is not an immunogen. Enzymes may lose activity over time or under harsh conditions [11, 12]. Moreover, many new or rare targets lack readily available BREs, and even when available, these BREs can also be slow, require high amounts of target material, or produce false positives [13]. Due to these issues, there is an increasing demand for stable, versatile and highly specific BREs like aptamers and peptides that can improve sensor performance and make biosensing more accessible [14].

Phage display technology is a powerful and versatile tool that plays a vital role in developing modern biosensors [15]. This technique involves using bacteriophages to display a wide variety of small proteins, such as peptides or antibody fragments, on their surfaces [15]. Biopanning is used to rapidly screen large libraries of these engineered phages to find specific peptides as BREs that bind strongly and selectively to a target of interest, such as a pathogen, toxin, or biomarker [7]. Among the commonly used phages in this technology are M13, T4, T7, and λ [16]. These phages are preferred because they remain stable under challenging environmental conditions, such as high temperatures or extreme pH levels [17–19]. This exceptional stability comes from the unique structural organization of the Ff phage (e.g. M13), which consists of a single-stranded circular DNA encapsulated by thousands of copies of the major coat protein pVIII arranged in a 5-fold helical symmetry (Fig. 1A). This tightly packed cylindrical protein shell acts as a protective barrier, shielding the viral genome from denaturation and degradation under stress [17]. Additionally, the minor coat proteins (pIII, pVI, pVII, and pIX) positioned at both ends of the filament further contribute to structural integrity (Fig. 1A) [17–19]. This makes them suitable for real-world biosensing applications where stability and reliability are essential [19, 20]. In biosensor development, the accuracy and sensitivity of detection largely depend on the quality of the BREs [21, 22]. Phage display enables the selection of peptides as BREs that are not only highly specific but also robust and cost-effective [23]. For instance, the filamentous M13 phage, which carries single-stranded DNA (Fig. 1A), has been widely used to generate peptides that can detect harmful bacteria, chemical toxins, or disease-related biomarkers [24]. Its unique architecture, being highly stable, genetically programmable, and multivalent, has established M13 as a versatile tool in both diagnostics and therapeutics [25]. In diagnostics, M13-based peptides and scaffolds have been widely applied in paper-based, electrochemical, and optical biosensors for rapid, cost-effective, and sensitive detection [26]. In therapeutics, M13 has enabled the development of monoclonal antibodies through phage display and is increasingly being explored as a platform for vaccines and targeted drug or gene delivery [27]. A growing body of literature suggests that diagnostic and sensing applications constitute the majority of M13-related studies, while therapeutic applications, particularly in antibody discovery and delivery systems, are also rapidly expanding. Overall, this has led to advances in areas such as nanobiosensing, early disease diagnosis, vaccine research, and targeted therapeutics [27].

During phage display biopanning, M13 bacteriophage libraries are exposed to specific targets or analytes to identify peptides that bind with high affinity and can eventually be developed as BREs [28]. However, the main challenge in biopanning is that the number of target-bound phages produced is low, which requires the subsequent effective amplification strategies to generate enough phages for further screening and analysis [29]. Additionally, selecting a purification method for amplified target-bound phage to remove contaminants, such as bacterial debris, is crucial to evaluate, as it can hinder the affinity binding between phages and targeted analytes [26, 30, 31]. Therefore, maximizing the target-bound phage yield in a scalable and reproducible manner is essential for phage display biopanning. It depends on several key factors [32], including (i) host cell density [32], (ii) duration of phage and host infection [32, 33], (iii) phage-to-bacteria ratio (Multiplicity of Infection, MOI) [32–34], and (iv) phage purification methods (Fig. 1B) [31]. However, current literature lacks comprehensive studies on these parameters. Many biopanning protocols have involved infecting the *Escherichia coli* host at standard bacterial densities with an optical density of 0.4–0.6 at 600 nm using M13 phage, without clearly demonstrating the effect of host cell concentrations on phage infection efficiency and the impact on the number of target-bound phage generated [35–39]. Another aspect of phage amplification is the infection or incubation time, which is often set arbitrarily, typically between 4 and 24 h, to allow phages to infect host cells and replicate, with minimal investigation into how this duration influences phage replication kinetics or overall amplification efficiency [38–40]. The multiplicity of infection (MOI), the ratio of phage numbers added to infect host cells, based on published studies, ranges from 0.001 to 100, but there is no consensus on their impact on amplification bias or phage enrichment efficiency [41–42]. At low MOI values (e.g. 0.001–1), each bacterial cell is typically infected by a single phage particle, minimizing phage amplification [41–44]. However, this can result in slower amplification due to limited initial infection. In contrast, high MOI values (e.g. 10–100) may lead to multiple phage particles infecting the same host, which can result in superinfection exclusion, a process in which a bacterium already infected with phage resists subsequent infections [33, 34, 45]. In this context, the filamentous M13 bacteriophage initiates infection by specifically binding to the F pilus on F^+ *E. coli*, which serves as its primary receptor and mediates phage genome entry into the host cell [46, 47]. This receptor-dependent mode of infection emphasizes phenomena such as superinfection exclusion, where prior occupation or alteration of the F pilus limits subsequent entry of the phage genome, ultimately reducing phage amplification [48, 49]. Optimizing MOI is therefore crucial to get a sufficient yield of phage during amplification. The purification using polyethylene glycol (PEG)/NaCl precipitation followed by centrifugation is one of the most common methods used to purify amplified phage particles. This approach works by reducing the solubility of the phages, allowing them to be collected from the culture supernatant [35, 37, 44]. While widely adopted, it can be time-consuming and may not always recover all the phages, particularly when working with low phage concentrations [37]. On the other hand, filtration offers a quicker alternative. It uses size-based separation to isolate phages from host cell debris and other impurities [50, 51]. Comparing these two methods is important to understand which one provides better phage yield and purity, especially when preparing samples for downstream applications like sequencing, binding assays, or biosensor development. A clearer picture of their efficiency could help improve the overall consistency and effectiveness of phage amplification workflows.

This study aims to investigate and optimize the phage display method to achieve efficient, reproducible, and large-scale amplification of M13 phages. The optimized conditions are expected to accelerate the application of phage display in biosensing and therapeutic development. Most importantly, our findings lay the foundation for identifying new and effective biorecognition elements that could transform diagnostic strategies across both biomedical and industrial

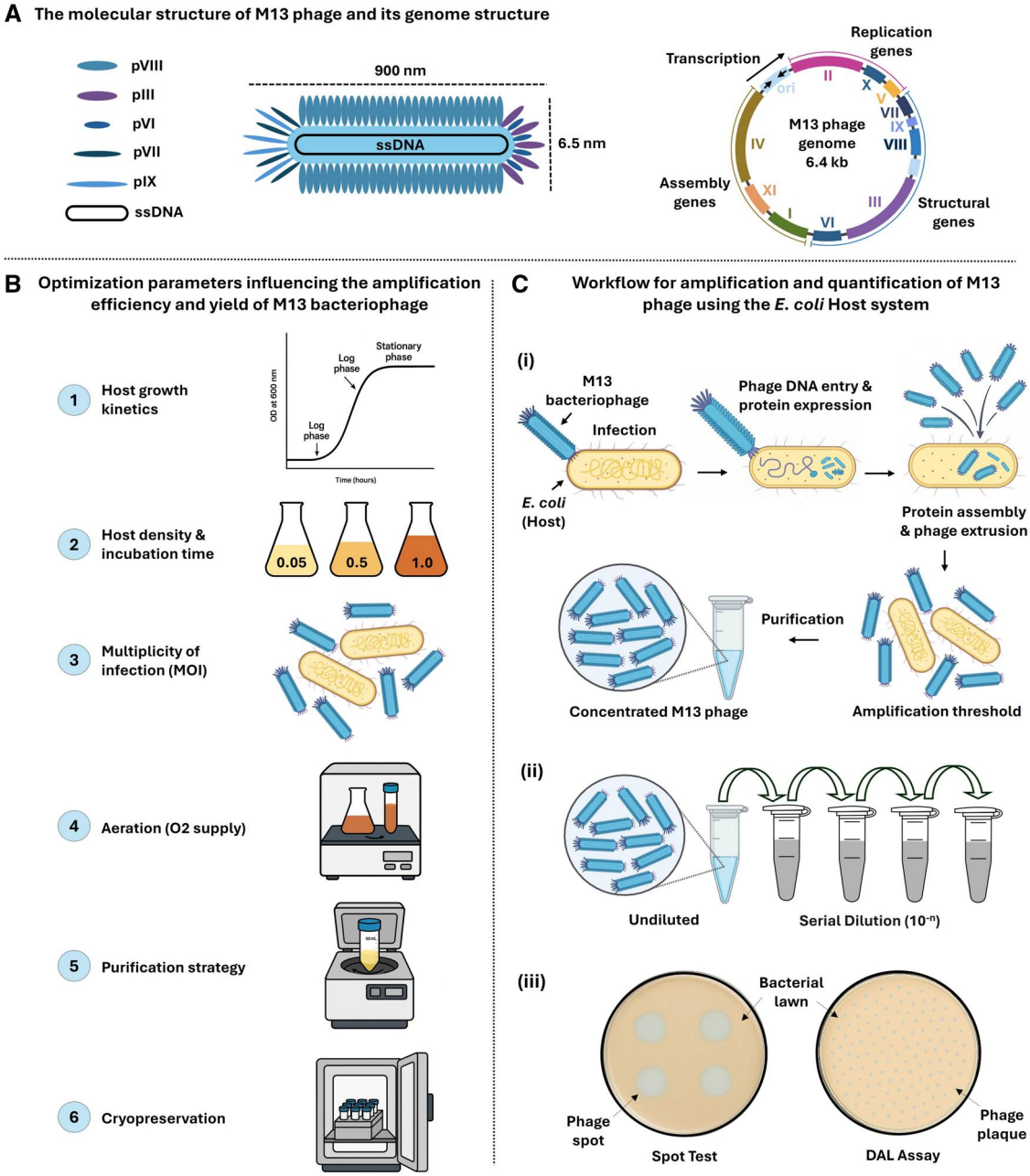

Figure 1 Molecular structure of M13 bacteriophage, key parameters for optimizing its amplification, and the workflow for amplifying and quantifying M13 in the *E. coli* host system. (A) The molecular structure of M13 phage and its genome organization. Left: schematic of the filamentous M13 virion (∼900 nm long, ∼6.5 nm wide) showing the major coat protein pVIII along the shaft and the minor coat proteins (pIII, pVI, pVII, pIX) at the tips surrounding the single-stranded DNA (ssDNA). Right: circular map of the ∼6.4 kb M13 genome highlighting genes involved in transcription/replication, assembly/secretion, and virion structure. (B) Optimization parameters influencing amplification efficiency and yield: (1) host growth kinetics; (2) host density and incubation time; (3) multiplicity of infection (MOI); (4) aeration (O_2 supply); (5) purification strategy; and (6) cryopreservation ('phage banking'). (C) Workflow: (i) M13 infects *E. coli*; phage ssDNA enters the cell, phage proteins are expressed, and virions assemble and extrude through the envelope without host lysis, enabling continuous production; amplified phage is harvested and concentrated by centrifugation. (ii) 10-Fold serial dilutions (10^{-n}) of the phage supernatant are prepared to obtain countable plaques. (iii) Detection and quantification are performed by a qualitative spot test (clearing of the bacterial lawn) and a double-agar layer (DAL) plaque assay for phage titre determination (PFU/ml).

sectors. Figure 1 represents a schematic overview of the molecular structure of M13 bacteriophage, key parameters and workflow comprising infection, amplification, and quantification, ensuring assessment and optimization of M13 phage propagation for effective biopanning and subsequent biosensor applications.

Materials and methodology

Escherichia coli strains and M13 phage

The bacterial strain used in this study was *E. coli* K-12 ER2738 strain (F′*proA*$^{+}$*B*$^{+}$ *lacI*^{q} Δ*(lacZ)M15 zzf::Tn*10(Tet^{R})/*fhuA2 glnV* Δ*(lac-proAB)*

thi-1 Δ*(hsdS-mcrB)5* (New England Biolabs, Australia). The bacteriophage M13 ATCC 15669 was provided by RMIT University.

Growth curve of *E. coli* K-12 ER2738

The growth curve of *E. coli* K-12 ER278 was established and plotted to determine the growth time and density of the *E. coli* population based on optical density at a wavelength of 600 nm (OD_{600}) and bacterial cell numbers in colony-forming units for subsequent phage infectivity experiments. The *E. coli* K-12 ER2738 was grown in Luria-Bertani (LB) broth overnight at 37 °C with constant orbital shaking at 100 rpm according to Mira *et al.* [52] A 2% *E. coli* inoculum was prepared by diluting the overnight culture to an optical density (OD) of 1.5 at 600 nm and mixing it with 5 ml of fresh LB to ensure a standardized and controlled starting cell density for experiments. The 2% *E. coli* culture grew at 37 °C with constant orbital shaking at 250 rpm. The OD values of the *E. coli* culture were measured using a PerkinElmer LAMBDA 365 UV/Vis Spectrophotometer from PerkinElmer, USA, at a regular 30-min interval until it reached a stationary plateau at 10 h of incubation. The OD_{600} values of *E. coli* were plotted against time (Fig. 2A). The bacterial growth curve was fitted using the Boltzmann sigmoidal equation, which effectively captures the typical S-shaped (sigmoidal) profile of microbial growth [53]. The general form of the Boltzmann equation is [54]:

$$y = \frac{A_1 - A_2}{1 + e^{\frac{x - x_0}{dx}}} + A_2$$

where y = OD_{600} (optical density at 600 nm), A_1 = initial (minimum) OD value (baseline), A_2 = final (maximum) OD value (plateau), x = time, x_0 = the time at which the growth rate is at its maximum (inflection point), dx = the time constant, related to the slope of the curve at the inflection point.

This model was used to fit the OD_{600} values plotted against time to quantify the growth phases of *E. coli*, including lag, log, and stationary phases. The sigmoidal fit provides insight into the transition points and allows for the precise determination of the growth rate and generation time under the tested conditions. The colony-forming units (CFUs) of *E. coli* were determined using the Trypan Blue dye exclusion assay [55–57]. Briefly, 1 ml of *E. coli* culture was harvested at OD_{600} of 0.05, 0.5, 1.0, and 1.5 and centrifuged at 5000×*g* for 10 min at 4 °C. The pellet was washed twice with Tris-buffered saline, TBS (50 mM Tris-HCl, pH 7.5, 150 mM NaCl) and resuspended again in 1 ml of TBS. The resuspended *E. coli* cells were diluted 10-fold in TBS. Each dilution of *E. coli* cells was mixed with an equal volume of 0.4% Trypan Blue. The 10 µl aliquot of Trypan Blue mixed culture was loaded onto a Neubauer chamber (0.1 mm depth, 0.0001 ml chamber volume). The number of viable bacterial cells in 12 out of 25 central grid squares was counted under the light microscope at 40X magnification, and the average cell count was used in the equation below to determine colony-forming units per millilitre (CFU/ml). The graph of CFU/ml of *E. coli* was plotted against the corresponding OD_{600} (Fig. 2B).

$$\text{CFU/ml} = \left(\frac{\sum_{i=1}^{n} N_i}{n} \times F\right) \times D \times 10^4$$

where N_i = Number of cells (CFU) counted in each selected square, n = Number of squares counted, F = Scaling factor to total squares in the grid (e.g. 25), D = Dilution factor, 10^4 = Conversion factor (from haemocytometer volume: 0.1 mm^3 = 10^{-4} ml).

Spot test assay

A rapid spot test assay was conducted according to previously described protocols with minor modifications to determine the viability of M13 phage in infecting and replicating within the host cells of *E. coli* K-12 ER2738, before quantifying the M13 phage population [58, 59]. To obtain early log phase *E. coli*, a 2% inoculum (OD_{600} ≈ 1.5) from an overnight culture was added to 5 ml fresh LB broth and

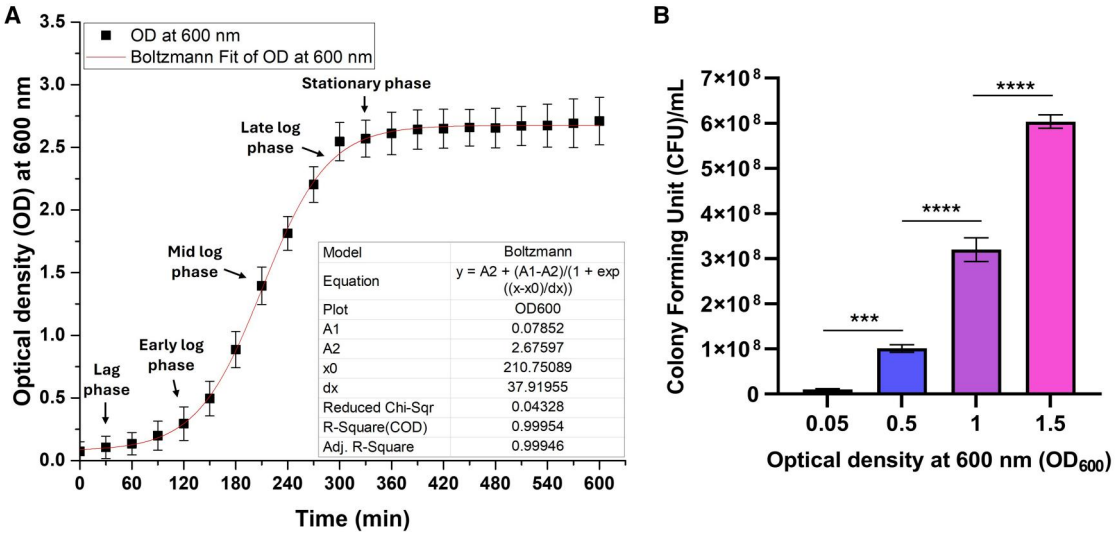

Figure 2 Growth kinetics of ER2738: Bacterial optical density (OD) over time and CFU count at different OD values. (A) Growth kinetics of *E. coli* ER2738 were measured as optical density (OD) at 600 nm over time. The experimental data are fitted using a Boltzmann sigmoidal curve with corresponding equation parameters shown in the inset table. (B) Colony-forming unit (CFU) counts at different OD_{600} values, indicating bacterial concentration at various growth phases. Error bars represent standard deviations from independent biological triplicate measurements. One-way ANOVA with Tukey's post hoc multiple comparison test showed significant differences among all OD_{600} groups (***$P < .001$, ****$P < .0001$)

incubated at 37 °C at 250 rpm until OD_{600} reached ∼0.5. One hundred microlitres of the early log phase *E. coli* culture was harvested and mixed with 3 ml of LB agar containing 0.7% (w/v) agar (soft agar), then uniformly overlaid on an LB agar (LA) solid agar plate. A 10 microlitre aliquot of phage suspension was applied to the solidified *E. coli* lawn culture on the LA plate and incubated overnight at 37 °C. The appearance of plaque-forming zones confirmed successful phage infection and replication in the *E. coli* host cells.

Double agar layer (DAL) assay and M13 phage titration

The DAL assay was used to quantify the M13 phage population and its propagation according to the previously published method, with slight modifications [39, 60, 61]. A bottom layer of 15 ml of LA agar was prepared. The early log phase *E. coli* culture for infectivity by M13 phage was prepared according to the spot test assay described above. The top layer, consisting of a mixture with 100 µl of early log phase *E. coli* cells, 200 µl of a 10-fold diluted M13 phage suspension in TBS, and 3 ml of 0.7% LA, was evenly overlaid on the bottom agar layer and incubated at 37 °C overnight. The clear plaque-forming zones were counted, and the plaque-forming units were calculated according to the following formula:

$$\text{Undiluted phage suspension per ml} = \frac{pfu_1 + pfu_2 + \cdots + pfu_n}{v_1 + v_2 + \cdots + v_n}$$

where

- *pfu*: number of plaques forming units from countable sample dilution plates
- *v*: volume used × dilution factor
- *n*: number of counts

And the standard deviation was calculated using the following formula:

$$S = \sqrt{\frac{1}{N-1}\sum_{i=1}^{N}(x_i - x)^2}$$

where

- S = standard deviation
- N = sum of sample
- x_i = sample value
- x = mean value

Additionally, phage particle concentration was measured using a PerkinElmer LAMBDA 365 UV/Vis spectrophotometer (PerkinElmer, USA) at 269 and 320 nm with a low-volume quartz cuvette. Phage particles were calculated using the previously reported equation to confirm DAL-based quantification [39, 62]:

$$\text{Phage particles/ml} = \frac{(6 \times 1016) \times (A269 - A320)}{N}$$

where

- N is the number of DNA bases in the M13 genome (6407 bases)

E. coli densities and incubation time for M13 phage-*E. coli* host interaction

To generate the desired plaque counts, the incubation time required for M13 phage to effectively infect and replicate in varying numbers of *E. coli* host cells was determined. A consistent M13 phage count of 2×10^9 PFU/ml was used to infect from early log phage to mid-log phase *E. coli* cells at OD_{600} nm with values of 0.05 (∼1×10^7 CFU/ml), 0.5 (∼1×10^8 CFU/ml), 1.0 (∼3×10^8 CFU/ml), and 1.5 (∼6×10^8 CFU/ml). The *E. coli* and M13 phage cell suspensions were mixed well in 20 ml LB broth in sterile 250 ml conical flasks to ensure sufficient aeration and incubated at 37 °C for 5 and 16 h, respectively. After incubation, the *E. coli* host cells were removed through centrifugation at 5000×*g* for 10 min at 4 °C. The supernatant containing the amplified M13 phages was then quantified using the DAL assay, as described in the 'Double agar layer (DAL) assay and M13 phage titration' section. The optimized infection time and the number of *E. coli* cells were applied for subsequent experiments.

Determine the multiplicity of infection (MOI) of M13 phage

The MOI of M13 phages were determined by testing various ratios of M13 phages to *E. coli* cells. The infectivity ratios of M13 phage to *E. coli* were evaluated at 1:1, 2:1, 5:1, 10:1, and 100:1, using 0.25×10^8 CFU/ml of *E. coli* host cells and a range of 0.25×10^8 PFU/ml to 25×10^8 PFU/ml of phages. Suspensions of *E. coli* and M13 phages were thoroughly mixed in 20 ml LB broth in sterile 250 ml conical flasks to ensure sufficient aeration and incubated at 37 °C with continuous orbital shaking at 250 rpm for 5 h. After incubation, the *E. coli* was removed by centrifugation at 5000×*g* for 10 min at 4 °C. The supernatant containing the amplified M13 phages was then quantified using the DAL assay, as described in the 'Double agar layer (DAL) assay and M13 phage titration' section.

The effect of aeration on M13 phage infection

The impact of aeration on *E. coli* host cell infection with M13 was evaluated using different container types and controlled orbital shaking speeds, as previously published in the literature, with modifications [39, 60, 61]. To independently assess the effect of container type on aeration, 20 ml of *E. coli* and M13 phage culture was grown either in sterile 50 ml polypropylene Falcon-type tubes, leaving ∼50% of headspace to constrain the air–liquid interface, and in 250 ml glass Erlenmeyer flasks, leaving ∼90% of headspace to maximize the oxygen transfer. All these experiments were performed at a fixed orbital shaking speed of 250 rpm. In parallel, to evaluate the effect of controlled shaking speed on aeration during phage–host infection, 20 ml *E. coli*–phage cultures were grown in sterile 250 ml glass Erlenmeyer flasks at 180, 250, and 320 rpm (same flask type throughout), thereby isolating the impact of shaking speed on oxygen transfer. In each aeration condition, the ratios of M13 phage to *E. coli* at 2:1, 10:1, and 100:1 were tested. The densities of M13 phage to *E. coli* were prepared according to the ratios: 0.5×10^8 PFU/ml: 0.25×10^8 CFU/ml, 2.5×10^8 PFU/ml: 0.25×10^8 CFU/ml, and 25×10^8 PFU/ml: 0.25×10^8 CFU/ml. Suspensions of *E. coli* host cells and M13 phages were

thoroughly mixed in LB and incubated at 37 °C with continuous orbital shaking as described above for 5 h. After incubation, the *E. coli* host cells were removed by centrifugation at 5000×*g* for 10 min at 4 °C. The supernatant containing the amplified M13 phages was then quantified using the DAL assay, as described in the 'Double agar layer (DAL) assay and M13 phage titration' section.

M13 phages recovery by filtration

To enhance the recovery of M13 phages from *E. coli* infection, filtration was performed after centrifuging the *E. coli* and phage suspensions following incubation, as outlined in the referenced method [50, 63]. After incubation with phages, *E. coli* host cells were removed via centrifugation as described in the '*E. coli* densities and incubation time for M13 phage-*E. coli* host interaction' section. The supernatant was subsequently filtered through three types of sterile 0.22 μm, 33 mm diameter syringe filters (Merck, Germany) to remove residual bacterial debris, yielding a clarified filtrate containing M13 phage particles. The filters evaluated were: Millex^{TM}-GP filter units (polyethersulfone [PES] membrane), Millex^{TM}-GS filter units (mixed cellulose ester [MCE] membrane), and Nylon 66 membrane filters (polyamide membrane). Filtration efficiency was then assessed to compare phage recovery across membrane types. This filtrate was subsequently diluted 10-fold in Tris-buffer saline (50 mM Tris-HCl, pH 7.5, 150 mM NaCl) and quantified using the DAL assay, as detailed in the 'Double agar layer (DAL) assay and M13 phage titration' section.

M13 phage recovery by PEG/NaCl precipitation and centrifugation

The recovery of M13 phages using polyethylene glycol (PEG) and sodium chloride (NaCl) precipitation followed by centrifugation was evaluated in comparison with filtration, as described in the 'M13 phages recovery by filtration' section. The PEG/NaCl precipitation was performed according to the previously published method [40, 61, 62]. After incubation with phages, *E. coli* host cells were removed via centrifugation, as outlined in the '*E. coli* densities and incubation time for M13 phage-*E. coli* host interaction' section. The supernatant was mixed with one-fifth volume of a 2.5 M NaCl/20% (w/v) PEG-8000 solution and incubated on ice for 1 h to precipitate phages. Subsequently, it was centrifuged at 20 000×*g* for 15, 30, or 60 min at 4 °C to pellet the phages to evaluate the effect of centrifugation time on phage recovery efficiency. The supernatant was then mixed with one-fifth volume of PEG/NaCl solution and incubated to precipitate phage particles independently for 1 h, 4 h, or overnight (16 h) at 4 °C, to assess the effect of PEG/NaCl incubation duration on phage recovery efficiency. The mixture was subsequently centrifuged at 20 000×*g* for 60 min at 4 °C to pellet the phage. Phage purification typically involves two rounds of PEG/NaCl precipitation to improve phage purity. The pellet was resuspended in Tris buffer saline (50 mM Tris-HCl, pH 7.5, 150 mM NaCl), diluted 10-fold, and quantified using the DAL assay, as described in the 'Double agar layer (DAL) assay and M13 phage titration' section. To assess bacterial contamination after purification, aliquots from unpurified phage suspensions and phage suspensions purified by PEG/NaCl precipitation followed by centrifugation were plated using the spread plate method on LB agar and incubated overnight at 37 °C [40]. Viable *E. coli* ER2738 colonies were counted and expressed as CFU/ml to evaluate purification efficiency.

Stability and viability of M13 phage

To determine the long-term stability and viability of M13 phage, a high-titre phage stock of approximately 1.8×10^{10} PFU/ml was prepared in 15% (v/v) glycerol by mixing an equal volume of the phage suspension with 30% glycerol [39]. For comparison, a higher-titre M13 stock ($\sim 3.4 \times 10^{11}$ PFU/ml) was also prepared and stored under identical conditions in 50% (v/v) glycerol. The phage stocks were stored at –80 °C for one year. After a year of storage, the frozen M13 phage stock was thawed on ice and diluted 10-fold in TBS buffer for viability testing. The diluted phage was quantified using DAL as described in the 'Double agar layer (DAL) assay and M13 phage titration' section.

Statistical analysis

Statistical analyses were conducted using GraphPad Prism (version 9.5, GraphPad Software, San Diego, CA, USA). Data are presented as means ± standard deviations from three independent replicates. Differences between experimental groups were evaluated using suitable statistical tests based on the experimental design: comparisons between two groups employed unpaired two-tailed Student's *t*-tests, while comparisons among multiple groups were analysed using one-way analysis of variance (ANOVA) followed by Tukey's post-hoc multiple comparisons test. Additionally, two-way ANOVA was used to analyse experiments involving two independent variables, such as aeration conditions and infection ratios. A significance level of $P < .05$ was considered statistically significant for all analyses, with significance denoted as $^{*}P < .05$, $^{**}P < .01$, $^{***}P < .001$, $^{****}P < .0001$ and no significance stars are shown for comparisons that were not statistically significant.

Results and discussion

Growth curve of *E. coli* ER2738

The growth curve of *E. coli* ER2738, depicted in Fig. 2, aligns closely with the Boltzmann sigmoidal model, achieving an R^2 of 0.9996. It shows typical bacterial growth, including a lag phase, a log phase at 120 min, and a stationary phase at 300 min. Research indicates that M13 phages infect *E. coli* most efficiently during the early log phase to mid-log phase, within the OD_{600} nm 0.05–1.5 range, when *E. coli* has active metabolism and vigorous DNA replication, which creates ideal conditions for phage replication [38, 64, 65]. In our experiment, *E. coli* cells were collected between the early log phase to mid-log phase for further phage infectivity studies. The viable cell count ranged from 1×10^7 to 6×10^8 CFU/ml at corresponding OD_{600} nm values, ensuring ample viable cells for effective phage infection (Fig. 2B). A significant correlation ($P < .0001$) was observed between optical density and viable cell count during the early to mid-log phase. The strong, consistent relationship between OD_{600} nm and viable cell counts allows for reliable scaling of phage production protocols, crucial for industrial or therapeutic uses requiring consistent bacterial input [66, 67]. After approximately 300 min post-inoculation, cultures entered the stationary phase, indicating the importance of avoiding late-phase cultures for infection, as diminished metabolic activity at this stage is less favourable for phage replication [68–70]. Overall, these results underscore the importance of host cell dynamics in optimizing M13 phage replication, highlighting that timing the infection to coincide with the host's early to mid-log phase can significantly improve phage yields.

Spot test and DAL assay confirm M13 phage infectivity, amplification, and quantification

Accurate detection and quantification of M13 phage are essential for evaluating phage amplification efficiency and viability, particularly in phage display applications [39]. Figure S1A demonstrates the initial assessment of M13 phage activity using the spot assay and the double agar layer (DAL) assay. The spot test assay provided rapid, visual confirmation of phage infectivity, evidenced by clear lysis zones on a bacterial lawn in undiluted samples. Although qualitative, the spot test effectively screens phage activity and infectivity across multiple samples [58, 59]. This method is critically important in phage display, as it provides immediate confirmation of phage viability and infectivity that helps to validate and select suitable phage candidates for further experimentation, including in phage library biopanning workflows [58, 59]. It enables rapid, visual screening of phage infectivity before proceeding to downstream selection (biopanning) steps. This ensures that only viable and infective phage clones are used, improving the efficiency and reliability of biopanning experiments. For quantitative analysis, the DAL assay provided clear, distinct plaques at dilutions of 10^{-6} and 10^{-7}, resulting in an estimated M13 phage titer of $\sim 3.56 \pm 0.45 \times 10^{9}$ PFU/ml, verifying the phage concentration in stock. Quantitative evaluation through DAL assays is crucial in phage display workflows, ensuring precise phage enumeration and reproducibility [28]. To further validate DAL-based quantification, phage concentration was also measured by UV–Vis spectrophotometry at 269 nm and 320 nm using a spectrophotometer with a low-volume quartz cuvette, and phage particles were calculated as described (Fig. S1B). Two independent phage concentrations were quantified using both methods, showing overall comparable titers between DAL and UV-based measurements. Notably, UV-derived values were slightly higher than DAL-based titers, which is expected because the DAL assay enumerates infective (viable) phage particles, whereas UV-based quantification estimates total particle concentration and may include non-infective particles or free nucleic acid/protein [71]. Nevertheless, the close consistency between the two approaches supports the reliability of the DAL assay for routine M13 phage quantification and strengthens confidence in its use throughout the study. By reliably quantifying phage titers, this method supports critical decision-making during phage display biopanning, amplification, storage, and purification processes, making it essential for generating consistent, high-quality phage stocks necessary for downstream applications [28, 29].

To further investigate initial phage propagation and amplification efficiency, we assessed phage recovery immediately after mixing phage with host bacteria (0 h) and following overnight incubation (Fig. S2). This experiment was included to establish a baseline reference for standard overnight M13 propagation and to confirm net production of viable phage before the optimization studies presented in the 'Effect of *E. coli* host density and incubation time on M13 phage amplification' to 'Aeration supports better phage infection' sections. Figure S2A (left) confirmed phage infectivity through the Spot test, visualized by clear bacterial lysis zones at lower dilutions. Simultaneously, DAL assays revealed distinct plaques at a 10^{-7} dilution (Fig. S2A, right), indicative of successful phage replication and amplification. Quantitative DAL analysis (Fig. S2B) showed a significant increase in phage titers from $\sim 7.12 \times 10^{8}$ PFU/ml at 0 h to $\sim 1.5 \times 10^{9}$ PFU/ml after overnight incubation, yielding a relative recovery ratio of 1:2.1 (Fig. S2C). Statistical evaluation using a two-tailed unpaired Student's t-test confirmed this increase was highly significant ($P < .0001$), highlighting overnight phage amplification facilitated by metabolically active log-phase *E. coli* hosts [40, 64, 72]. Ultimately, the purpose of this experiment was to confirm that M13 phage amplifies in broth culture following infection of *E. coli*, resulting in successful enrichment of M13 phage particles quantified by the DAL assay. This baseline amplification assessment then guided our subsequent optimization of MOI, incubation time, and aeration in the 'Effect of *E. coli* host density and incubation time on M13 phage amplification' to 'Aeration supports better phage infection' sections. Thus, these findings emphasize the critical importance of the DAL assay as a reliable method for accurate quantification of M13 phage titers in phage display experiments [39, 60, 61]. The precision and reproducibility of plaque enumeration facilitated by serial dilutions within the DAL assay ensure consistent quantification, which is essential in phage display applications for evaluating amplification efficiency, optimizing storage conditions, and verifying purification protocols [39, 60, 61]. Together, the spot test and DAL assay create a robust detection and quantification pipeline that is indispensable in preparative workflows requiring consistent, high-titer phage stocks. Consequently, their integrated use significantly enhances the reliability and efficiency of phage display-based biosensing, diagnostic, and therapeutic applications.

Effect of *E. coli* host density and incubation time on M13 phage amplification

To maximize M13 phage amplification efficiency and achieve a high plaque count, the effects of *E. coli* density and incubation time on their interactions were investigated [39]. *E. coli* cultures were collected at different OD_{600} at 0.05, 0.5, 1.0, and 1.5, spanning from early log through mid-log growth phases, to optimize phage infection. Before infection, a quick spot test confirmed M13 phage viability, and titration measured the PFU/ml count, which was around 1.5×10^{9} (Fig. S2). As shown in Fig. 3 and Fig. S3, after 5 h of incubation, the highest plaque counts of 1.2×10^{13} PFU/ml were observed using *E. coli* at OD_{600} of 0.05, corresponding to the start of the early log phase. Following this, 7×10^{12} PFU/ml was recorded as the second highest at the early log phase of OD_{600} of 0.5. The two-way ANOVA followed by Tukey's multiple comparisons test confirmed highly significant differences ($P < .0001$) between phage titers obtained at lower densities (OD 0.05 and 0.5) and higher densities (OD 1.0 and 1.5). These results emphasize the critical importance of initiating phage amplification at optimal bacterial densities (OD 0.05 to 0.5) for maximum yield [39, 73]. A similar observation was made during 16 h of incubation of M13 phage and *E. coli* cells, in which the elevated plaque counts were observed from the beginning and across the early logarithmic phase. In fact, filamentous M13 phage replicates most efficiently while infecting F^{+} *E. coli* cells in the early logarithmic phase of growth, when the bacteria are actively dividing. During this stage, the host's cellular machinery is highly active, supporting the processes essential to the M13 life cycle, including genome replication, coat protein synthesis, virion assembly, and continuous extrusion of phage particles without host lysis [39]. Our findings clearly demonstrate that initiating infection during this early log phase provides the most favourable physiological conditions for phage DNA replication and particle formation, resulting in prominently higher phage titers. While most established amplification protocols employ *E. coli* cultures with optical densities between 0.05 and 0.6 (OD_{600}), few have

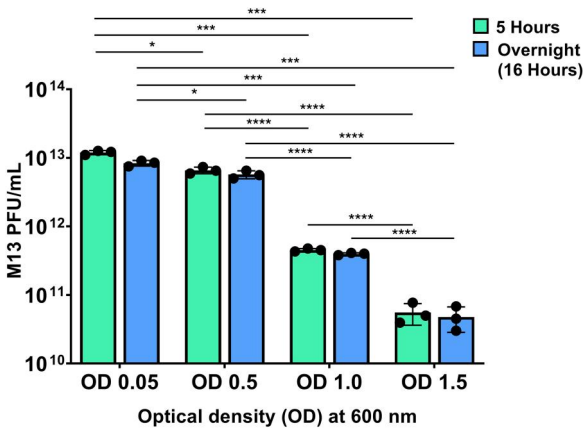

Figure 3 Optimization of M13 phage amplification at different host bacterial densities and incubation times. Quantification of M13 phage titers (PFU/ml, log10 scale) for different *E. coli* host OD values, comparing amplification for 5 h vs. 16 h. Each data point represents independent biological replicates. Error bars indicate standard deviation. Statistical analysis using two-way ANOVA followed by Tukey's multiple comparisons test revealed significant differences in M13 phage titers across host bacterial densities, with lower OD_{600} values (0.05 and 0.5) yielding significantly higher phage titers compared to higher ODs (1.0 and 1.5) (*$P < .05$, ***$P < .001$, ****$P < .0001$, as indicated). There was no significant difference in phage titers between 5 and 16 h of amplification ($P > .05$). Error bars represent standard deviations from independent biological replicates ($n = 3$)

explored how variations in host cell concentration affect infection efficiency and overall phage yield [35–38]. Although the precise molecular mechanisms behind this enhancement remain unclear, our results suggest that early log–phase cells allow the phage to harness the host's biosynthetic capacity more effectively, enabling faster genome replication, protein synthesis, and virion assembly. These findings are consistent with multiple studies that demonstrate a direct connection between bacterial growth phases and phage yield [66–68]. The referred studies support the assumption that optimal bacterial physiological state is a key determining factor of phage production efficiency. When the *E. coli* density entered the mid-log phase at OD_{600} 1 and 1.5, the plaque count decreased by one log and 2 logs, respectively. While OD_{600} values of 1.0–1.5 indicate the mid-logarithmic phase of *E. coli* growth when cells are usually dividing rapidly, the observed M13 phage yields at these levels were notably lower (Fig. 3). This unexpected result may result from multiple limiting factors, including high bacterial cell densities that likely accelerate nutrient and oxygen depletion [69, 70, 74], impairing cellular metabolism and limiting resources needed for phage replication and release [74]. Additionally, overcrowded conditions might hinder M13 phage release due to membrane stress and extracellular phage buildup. Receptor availability may also decrease since F pilus expression can decline under high-density or stressed conditions, such as nutrient limitation and oxygen deficiency [31, 68]. Similarly, starting infections at low OD with fast-growing bacteria helps many obligately lytic phages (i.e. T4) because rapidly dividing cells give the phage more resources: the latent period (time from infection to lysis) gets shorter and the burst size (phage per lysed cell) gets bigger. By contrast, when cultures get dense and oxygen/nutrients run low, phage development slows and total yield drops [67, 75, 76]. In temperate phages like lambda (λ), whether the phage chooses to lyse the host or integrate into the host genome (lysogeny) depends on the phage-to-host ratio (MOI) and the physiological condition of the host [77]. When the host is growing slowly, such as under nutrient limitation or low oxygen, the phage is more likely to enter lysogeny [78]. This reduces the number of cells that lyse and leads to lower production of free phage. This is because slow-growing cells have less ATP, which stabilizes a regulatory protein called CII [79]. Stable CII favours lysogeny over lysis [80]. Therefore, in high-density or poorly aerated cultures, even though many infections occur, phage yield may be low.

Long incubation from 5 to 16 h did not significantly increase phage titers at optimal bacterial densities, indicating that maximum amplification was reached within the first 5 h. This saturation is likely due to the rapid depletion of host cellular resources and replication machinery during the exponential growth phase [67, 81]. Once the bacterial growth moved into the stationary phase, lack of nutrients and slower metabolism reduced phage production [64, 81]. Extended incubation did not improve infection efficiency, likely due to the accumulation of metabolic by-products and increased competition for nutrients, indicating that shorter incubation periods are more efficient. Moreover, overnight incubation at the highest bacterial density tested (OD_{600} = 1.5) slightly reduced phage yield (Fig. 3), reflecting the minor negative impact of long incubation. However, no significant difference in phage titers was observed between 5 and 16 h of amplification. Overall, these findings establish guidelines for optimizing M13 phage amplification, highlighting the beginning of infection during the lag to early-logarithmic phase (OD 0.05–0.5) and 5 h incubation durations to enhance efficiency and yield, which is crucial for effective phage display library amplification. Notably, these findings are broadly consistent with workflows such as the New England Biolabs (NEB) Phage Display Peptide Library Kit [38]. We acknowledge that amplification conditions can vary across self-constructed phage display libraries; for example, infections are often initiated with *E. coli* TG1 at OD_{600} ~0.3–0.6, and amplification is frequently performed overnight [82].

Multiplicity of infection (MOI)

A constant concentration of *E. coli* at 0.25×10^8 CFU/ml was infected with M13 phages to host *E. coli* at the ratios of 1:1, 2:1, 5:1, 10:1, and 100:1. The growth curve of *E. coli* without phage infection showed a standard sigmoidal growth pattern, reaching an optical density (OD_{600}) plateau of approximately 2.5 at around 360 min (Fig. 4A). In contrast, bacterial growth was significantly reduced in phage-infected cultures, and most inhibition was observed at the moderate phage-to- *E. coli* ratio (2:1), followed by 5:1, 1:1, and 10:1. Conversely, at the highest phage concentration (phage: *E. coli* ratio of 100:1), the bacterial growth curve closely resembled that of the curve of the uninfected *E. coli*, indicating minimal growth inhibition. At 5 h post-infection, the optical density (OD_{600}) measurements revealed an inverse relationship between host growth and M13 amplification efficiency (Fig. 4A; Table 1). Uninfected *E. coli* cultures reached an OD_{600} of ~2.53, while infected cultures displayed progressively lower OD values with increasing phage-to-host ratios from ~2.33 at 100:1, ~1.96 at 10:1, ~1.38 at 1:1, ~1.15 at 5:1, to ~0.27 at 2:1. The reduction in OD at the 2:1 ratio indicates substantial growth interference by phage infection, corresponding to the highest measured phage titer ($\sim 8.3 \times 10^{11}$ PFU/ml; Fig. 4B). This inverse correlation demonstrates that efficient phage amplification is associated with lower host density and phage infection with the host from early-log-phase, consistent with the findings in the 'Effect of *E. coli* host density and incubation time on M13 phage amplification' section (Fig. 3).

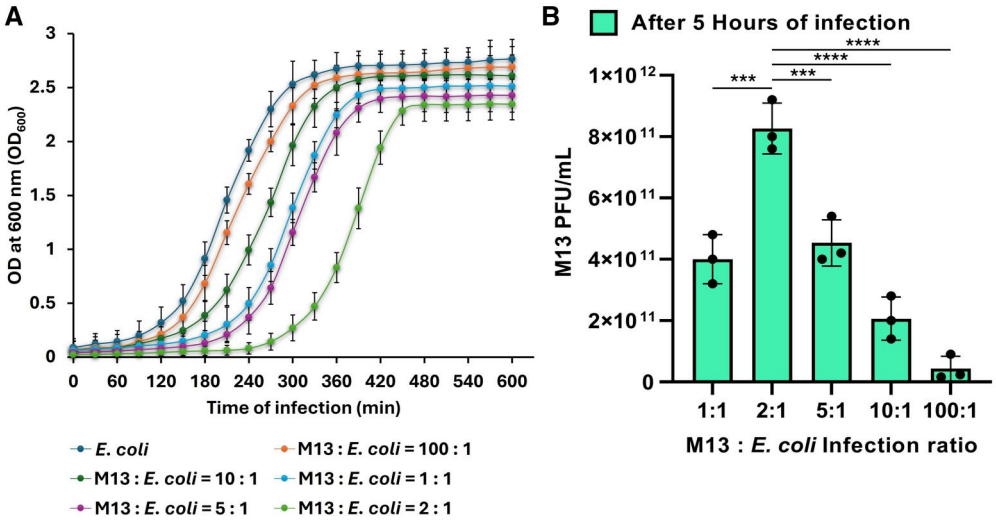

Figure 4 Effect of M13 phage to *E. coli* infection ratio on M13 phage amplification. (A) Growth curves of *E. coli* alone and *E. coli* infected with M13 at different infection ratios, measured by OD_{600} over time. Higher phage concentrations slow bacterial growth. (B) Quantification of M13 phage titers (PFU/ml) after 5 h of infection at different infection ratios. Each data point represents independent biological replicates ($n = 3$), and error bars indicate standard deviation. One-way ANOVA analysis revealed a statistically significant effect of infection ratio on M13 amplification (***$P < .001$, ****$P < .0001$), with the 2:1 ratio producing the highest phage yield

Table 1 Comparison of key factors influencing M13 amplification at low vs high MOI.

Factor	Effect at low MOI (e.g. 2:1)	Effect at high MOI (e.g. 10:1, 100:1)
Phage genome entry	Gradual infection, allows multiple productive cycles	Rapid adsorption to most cells; effective entry of phage genome may be reduced due to adsorption saturation
Superinfection exclusion (SIE)	Minimal or delayed	Likely contributes, but not exclusively; may limit subsequent productive infections
Phage-resistant mutants	Limited selection pressure	Increased selective pressure may accelerate emergence or enrichment of resistant mutants
Phage amplification	High, sustained production	Reduced due to combined effects of SIE, reduced adsorption efficiency, and possible resistance
Host growth (OD_{600})	Partially suppressed by active phage replication	Sustained growth despite infection, consistent with non-lytic M13 lifecycle
Overall phage yield	Maximal at M13: *E. coli* = 2:1	Significantly reduced despite high initial phage input

Conversely, higher ratios (10:1 and 100:1) resulted in elevated OD_{600} values but reduced plaque counts, implying diminished infection efficiency. However, DAL assays conducted after 5 h of infection further confirmed these observations (Fig. S4). Visual inspection of plaques revealed differences in phage yield, with the 2:1 infection ratio showing the highest plaque density. Quantitative results (Fig. 4B) confirmed these observations, as the 2:1 ratio significantly outperformed all other tested ratios, yielding approximately $\sim 8.3 \times 10^{11}$ PFU/ml. Higher ratios (10:1) produced markedly fewer phages ($\sim 2 \times 10^{11}$ PFU/ml), while ratios exceeding 5:1 showed reduced yields, supporting the idea that extreme infection ratios negatively impact phage production efficiency. Notably, the highest phage-to-host ratio (100:1) resulted in minimal bacterial growth inhibition (Fig. 4A) and a significant decrease in phage production (Fig. 4B). One possible explanation for this effect is superinfection exclusion (SIE). Superinfection exclusion (SIE) is a protective mechanism employed by the bacteria upon infection by the bacteriophage, which prevents subsequent phage infections [83]. At high multiplicities of infection (MOI), although M13 is initially abundant, phage amplification drops significantly, while optical density (OD_{600}) increases due to sustained bacterial growth (Fig. 4B). We assume that this outcome may be a result of superinfection exclusion (SIE) mediated by M13-encoded proteins, particularly pIII [84, 85]. This leads to the proposal that the pIII protein may be responsible for conferring superinfection immunity in M13-infected cells. Although superinfection exclusion (SIE) is a plausible contributor to the reduced M13 yield observed at very high phage-to-host ratios, it is not likely to be the sole explanation. At extreme MOI, multiple phage particles can adsorb to the same cell, which may reduce the effective entry of the phage genome or adsorption efficiency due to adsorption-driven perturbations of host physiology and a decreased probability of the genome entry per adsorbed phage [48]. In addition, high MOI can increase selective pressure on the bacterial population, potentially accelerating the emergence and enrichment of phage-resistant mutants (e.g. F pilus-associated changes), which

would further reduce productive infection and apparent phage amplification yield [49]. As a result, infected host cells enter a phage-resistant, but metabolically active state, where new productive infections are blocked, but cellular functions remain intact [83]. Consequently, even with diminished phage yield, OD_{600} continues to rise, reflecting the non-lytic nature of M13 and the survival of infected *E. coli* [84]. Statistical analysis using one-way ANOVA confirmed that the infection ratio significantly affected phage amplification ($P < .0001$), with the 2:1 ratio providing optimal conditions for maximal phage yield. On the other hand, at the low, 1:1 infection ratio, phage amplification yielded approximately 4×10^{11} PFU/ml after 5 h (Fig. 4B). This result suggests that while the infection efficiency was sufficient to initiate active M13 propagation, the overall yield was limited by the relatively lower initial phage input compared to the 2:1 ratio. However, the lower phage density reduces the frequency of infection events. Similar outcomes have been reported for other filamentous and ssDNA phages, where low multiplicity of infection (MOI) conditions result in slower amplification kinetics due to limited initial infection coverage of the host population [41–44]. These findings underscore the importance of precisely balancing phage-to-host ratios, highlighting that excessive phage inputs can unexpectedly diminish overall amplification efficiency. These findings reveal a dose-dependent switch in M13 infection outcomes, while moderate MOI favours robust phage amplification, high MOI induces early SIE that protects host cells at the cost of phage productivity. Thus, optimal phage amplification for practical applications should leverage moderate infection ratios, as demonstrated by the 2:1 condition, which maximizes both phage yield and bacterial host utilization. A summary is presented in Table 1.

Aeration supports better phage infection

Aeration plays a critical role in bacterial culture growth and phage propagation, significantly impacting M13 phage amplification efficiency. To evaluate the impact of aeration on M13 phage amplification, infections were performed at three phage-to-host ratios (M13: *E. coli* = 2:1, 10:1, and 100:1) under different culture container types and independently controlled orbital shaking speed, followed by quantitative plaque analysis (Fig. 5, Fig. S5). First, to independently assess container-dependent aeration effects on phage yield, experiments were conducted at a fixed orbital shaking speed (250 rpm) using 50 ml polypropylene Falcon-type tubes filled to ∼ 50% of their volume with 20 ml of culture to reduce the air-liquid interface, and using 250 ml glass Erlenmeyer flasks containing 20 ml of culture (∼ 90% headspace) to maximize the surface area for oxygen transfer (Fig. 5A, Fig. S5B). Under identical orbital shaking conditions, cultures grown in 250 ml glass Erlenmeyer flasks consistently produced significantly higher M13 titers than those grown in 50 ml polypropylene Falcon-type tubes across all infection ratios (Fig. 5B). At the 2:1 infection ratio, plaque counts increased from $\sim 2.0 \times 10^{11}$ PFU/ml (50 ml polypropylene Falcon-type tubes) to $\sim 8.3 \times 10^{11}$ PFU/ml (250 ml glass Erlenmeyer flasks), representing an approximate 315% increase. Similar, though less evident, increases were observed at 10:1 (∼ 43% increase) and 100:1 (∼ 72% increase), suggesting that improved aeration consistently facilitates higher phage replication. In addition, the culture container material itself is an important factor, as polypropylene tubes may contribute to reduced phage yield. Consistent with previous reports, our results demonstrate that phage propagation is influenced by container composition, with polypropylene surfaces

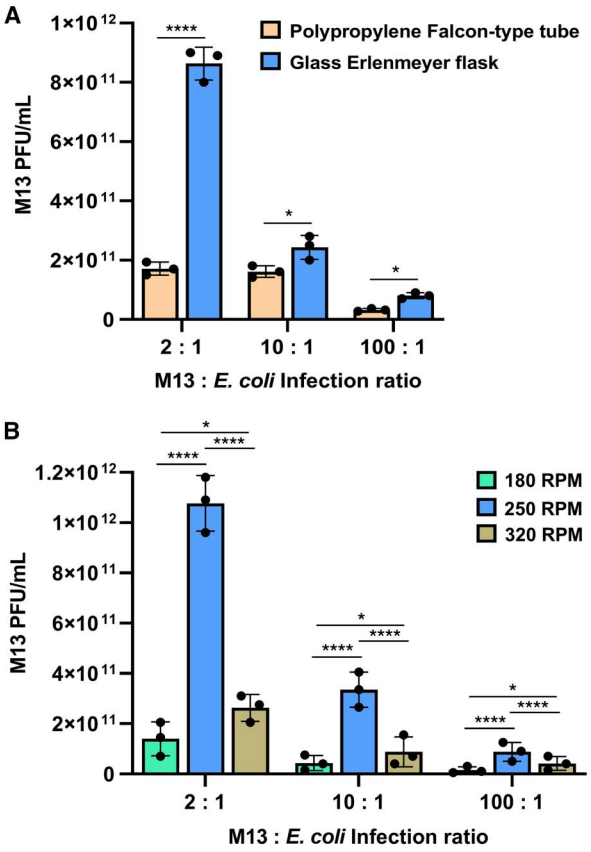

Figure 5 Effect of aeration on M13 phage amplification for 5 h under varying container types and shaking speeds across different phage-to-host infection ratios. (A) Comparison of M13 phage titers obtained after 5 h of infection using different container types at a fixed shaking speed (250 rpm): 50 ml polypropylene Falcon-type tubes versus 250 ml glass Erlenmeyer flasks. (B) Quantification of M13 phage titers (PFU/ml) following 5 h of infection at M13: *E. coli* ratios of 2:1, 10:1, and 100:1 under different shaking speeds (180, 250, and 320 rpm) in 250 ml glass Erlenmeyer flasks. Bars represent mean PFU/ml, with individual data points shown as dots and error bars indicating standard deviation from independent biological replicates ($n = 3$). Statistical significance was determined using two-way ANOVA followed by Tukey's multiple comparisons test; significance levels are indicated as (*$P < .05$, ****$P < .0001$)

associated with phage adsorption and reduced recovery [86]. Across all tested infection ratios, cultures grown in glass Erlenmeyer flasks consistently yielded higher M13 titers than those propagated in polypropylene Falcon-type tubes (Fig. 5A), indicating that container material may contribute to differences in apparent phage recovery, likely due to surface-associated adsorption or loss in polypropylene containers. When glass Erlenmeyer flasks consistently yielded higher M13 titers, we next fixed the container type (glass) and examined how oxygen transfer driven by different shaking speeds influences phage yield. As shown in Fig. 5B, increasing shaking speed significantly enhanced M13 phage amplification across all tested infection ratios. At the optimal infection ratio of 2:1, phage titers increased prominently with increasing aeration, reaching a maximum at 250 rpm ($\sim 1.1 \times 10^{12}$ PFU/ml), compared to lower yields at 180 rpm ($\sim 1.2 \times 10^{11}$ PFU/ml) and 320 rpm ($\sim 2.5 \times 10^{11}$ PFU/ml). Similar trends were observed at infection ratios of 10:1 and 100:1, where intermediate shaking (250 rpm) consistently produced higher phage

yields than either lower or higher shaking speeds. These results showing enhanced M13 phage amplification with increased aeration are consistent with previous findings that dissolved oxygen concentration and agitation rates influence filamentous phage yield in controlled culture systems [87]. On the other hand, excessive agitation (such as 320 rpm) and associated mechanical shear stress are known to affect phage stability and phage-host interactions [88]. Mechanical forces, such as shear, can influence phage structural integrity and adsorption dynamics, potentially reducing productive infection under high agitation conditions [88]. Two-way ANOVA confirmed a highly significant effect of shaking speed on phage yield ($P < .0001$), highlighting aeration (oxygenation) as a critical determinant of M13 amplification efficiency. Importantly, while the container type was held constant, increasing shaking speed within glass Erlenmeyer flasks resulted in a noticeable enhancement of M13 yield (Fig. 5B), demonstrating that aeration is an important factor in phage amplification. Collectively, these findings suggest that although container material likely contributes to overall phage recovery, improved aeration achieved through appropriate container types and controlled orbital shaking conditions is an important determinant of M13 phage amplification, as supported by two-way ANOVA, which shows a highly significant effect of aeration on phage yield ($P < .0001$). Improved aeration has been shown to positively influence microbial metabolism, and by extension, bacteriophage replication, including M13 [62]. Although direct studies on M13 phage amplification under varying oxygen conditions are limited, existing research supports the hypothesis that oxygen availability enhances host bacterial activity, which is critical for efficient phage replication. For instance, increased oxygen supply significantly improved metabolic fluxes and growth in *Azotobacter vinelandii*, suggesting that similar effects would benefit *E. coli*, the host for M13 phage [89]. Enhanced aeration was also found to improve bacterial nutrient uptake and phosphorus removal efficiency in wastewater systems, highlighting the metabolic sensitivity of microorganisms to dissolved oxygen levels [90]. Additionally, oxygen access influenced membrane protein orientation and accessibility in M13 major coat protein mutants, further underlining the importance of oxygen-related dynamics in phage biology [91]. Studies on other systems, such as microbially induced calcite precipitation and aquaculture, also demonstrate that sufficient aeration improves microbial performance and product output, which can be extrapolated to suggest enhanced phage replication efficiency under optimal oxygen conditions [92, 93]. Visual comparison of plaque formation under suboptimal (low shaking speed or use of polypropylene Falcon-type tubes) and optimal aeration (moderate shaking speed of 250 rpm in glass Erlenmeyer flasks) further supported these findings (Fig. S5**)**, showing notably increased plaque densities under optimal aeration conditions. Optimal aeration conditions likely enhanced bacterial metabolism and host replication efficiency, thereby improving the resources available for M13 phage replication. Overall, these results emphasize that aeration is a crucial, often underestimated factor for M13 phage amplification. While maintaining optimal *E. coli* host density and an appropriate multiplicity of infection (MOI) are essential for initiating efficient phage–host interactions, these parameters alone cannot ensure high phage yield without sufficient oxygen availability. Adequate aeration upholds the host's metabolic activity, ensuring continuous ATP generation and biosynthetic fluxes required for phage genome replication, protein synthesis, and virion extrusion [70]. In contrast, limited oxygen leads to metabolic slowdown, nutrient imbalance, and accumulation of toxic by-products, all of which restrict phage propagation [70]. Therefore, maximizing M13 phage amplification requires a balanced integration of host density, infection ratio, and aeration, where proper oxygenation maintains the physiological state of *E. coli* necessary for sustained, high-efficiency phage production. These findings highlight the importance of carefully optimizing aeration conditions, particularly for phage display applications, to ensure efficient and reproducible phage amplification.

Purification

To ensure contamination-free phage preparations, multiple researchers have employed 0.22 μm filtration units [50, 51]. Though other types, such as 0.45 μm filters, are useful for clarification or filtration, studies have shown that purification efficiency is often similar between 0.22 μm and 0.45 μm pore sizes [94]. However, we selected 0.22 μm filters for purification due to their smaller pore size, which provides better retention of bacteria and fine debris. Therefore, we evaluated the efficacy of 0.22 μm filtration for purifying amplified M13 phage suspensions, using *E. coli* cultures infected at the early logarithmic phase with an initial phage concentration of approximately 2×10^9 PFU/ml. Amplified M13 phage supernatants were filtered using three sterile 0.22 μm, 33 mm diameter syringe filter types: polyethersulfone (PES, Millex^{TM}-GP), mixed cellulose ester (MCE, Millex^{TM}-GS), and Nylon 66 (polyamide) membranes. Non-filtered supernatant served as a control. Filtration efficiency was assessed by plaque assay (DAL method) to quantify phage recovery following filtration. Figure 6Ai displays representative DAL assay plates for phage suspensions diluted to 10^{-9}, with and without filtration. Visual inspection of the respective plates indicates a substantial reduction in plaque numbers following filtration across all membrane types when compared to the non-filtered control, suggesting significant phage removal. Quantitative analysis (Fig. 6Aii) revealed a statistically significant decrease ($P < .0001$) in M13 phage titers post-filtration. Specifically, the non-filtered phage suspension exhibited titers of approximately 10^{13} PFU/ml, whereas filtration through PES, MCE, and Nylon 66 membranes resulted in titers of approximately 10^{11}, 10^{11}, and 10^{10} PFU/ml, respectively, equivalent to an overall 2-log reduction in recoverable phage particles. Among the membranes tested, PES filters exhibited the highest phage recovery, followed by MCE, while Nylon 66 filters showed the greatest loss of phage particles. These differences are likely due to fundamental differences in membrane surface chemistry and nonspecific adsorptive interactions; nylon membranes typically show higher protein- and particle-binding capacity, whereas PES membranes are widely recommended for biological sample filtration because they typically exhibit low protein/biomacromolecule adsorption and extractables, reducing loss of analytes such as proteins or virus particles [95, 96]. The considerable loss in phage particles indicates that it inadvertently traps a significant fraction of the M13 phage particles, substantially lowering phage yields. This may be attributable to phage aggregation or adherence to filter membranes [51]. Furthermore, the extended filamentous structure of M13 phage, which can reach lengths of approximately 900 nm [60], inherently challenges its passage through 0.22 μm pore-size filters, despite its narrow diameter (~6.5 nm). Although filtration effectively removes bacterial debris and enhances purity, an advantage for target-binding specificity in phage display, it also results in significant phage loss. This loss may include high-affinity binders,

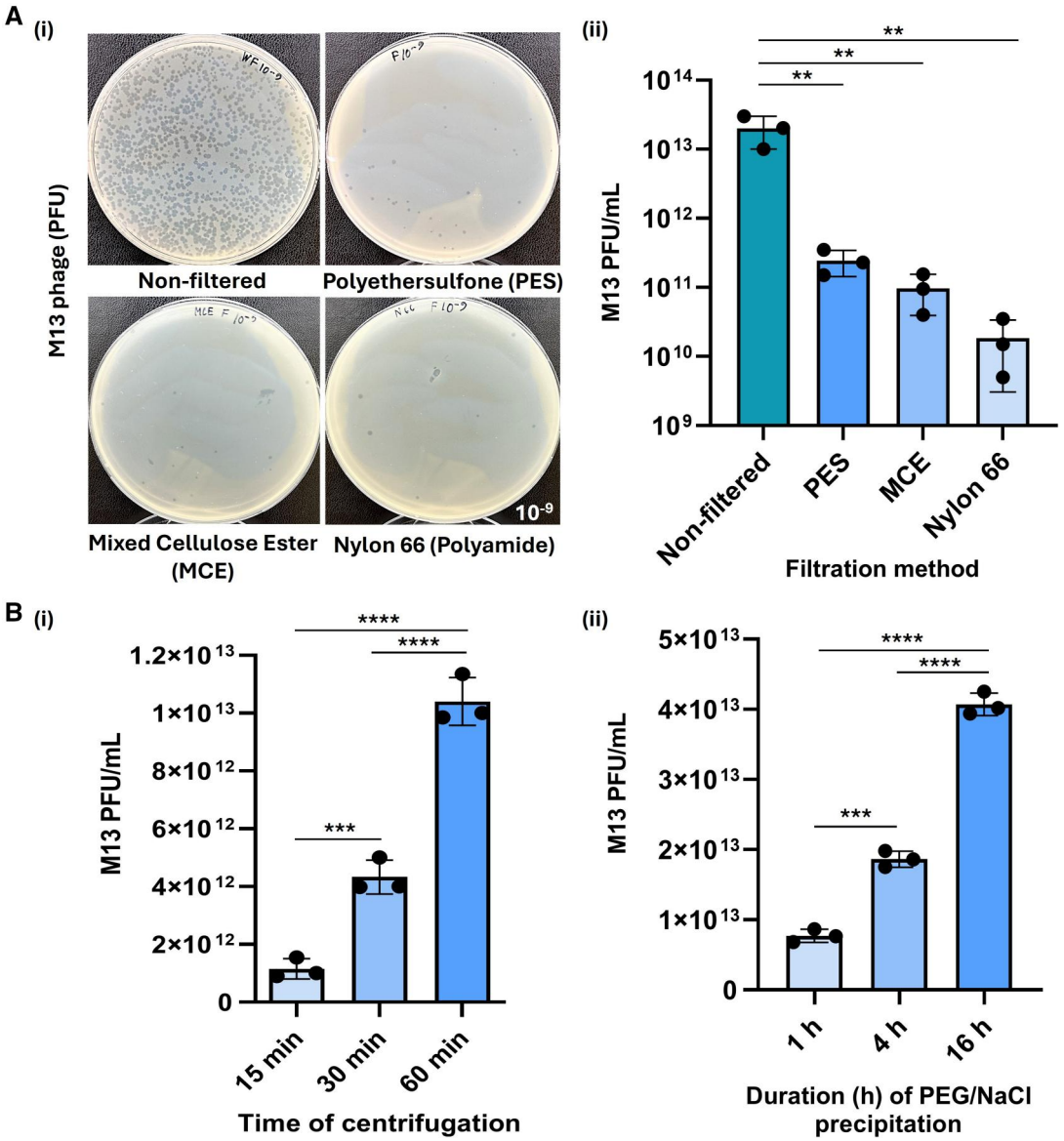

Figure 6 Optimization of M13 phage purification: effects of membrane filtration, PEG/NaCl precipitation duration and centrifugation time. (A) Effect of membrane filtration on M13 phage recovery. (i) Representative plaque assay plates (PFU) showing M13 phage titers at a 10^{-9} dilution under different filtration conditions: non-filtered, polyethersulfone (PES), mixed cellulose ester (MCE), and nylon 66 (polyamide) membranes. (ii) Quantification of M13 phage titers (PFU/ml) following filtration using different membrane types. Non-filtered samples yielded significantly higher phage titers compared to filtered samples, with membrane-dependent differences observed. (B) Optimization of PEG/NaCl precipitation and centrifugation parameters. (i) Effect of centrifugation time (15, 30, and 60 min) on M13 phage recovery following PEG/NaCl precipitation for 1 h, showing a progressive increase in phage yield with longer centrifugation times. (ii) Effect of PEG/NaCl precipitation duration (1, 4, and 16 h) on M13 phage recovery at 60 min of centrifugation at 20 000×g, with significantly higher titers observed after extended precipitation times. Bars represent mean PFU/ml, individual data points are shown as dots, and error bars indicate standard deviation from independent biological replicates ($n = 3$). Statistical significance was determined using one-way ANOVA with Tukey's multiple-comparison tests, as indicated in the figure (**$P < .01$, ***$P < .001$, ****$P < .0001$)

potentially undermining the diversity and quality of the amplified phage pool during phage display application.

We next investigated the effect of PEG/NaCl precipitation combined with different precipitation and centrifugation times. During this step, bacteria and bacterial debris were removed through repeated moderate-speed centrifugation, pelleting only the bacteria and collecting the supernatant containing the phage. This process ensured the effective elimination of bacterial contaminants, preventing any residual debris from remaining. To optimize recovery following PEG/NaCl precipitation, we evaluated the effects of centrifugation duration and PEG/NaCl precipitation time on M13 yield (Fig. 6B; Fig. S6). When phage suspensions were precipitated for 1 h and centrifuged at 20000×*g*, increasing the centrifugation time from 15 to 30 and 60 min produced a progressive and significant increase in recoverable titers, rising from approximately $\sim 1 \times 10^{12}$ PFU/ml (15 min) to $\sim 4 \times 10^{12}$ PFU/ml (30 min) and $\sim 1 \times 10^{13}$ PFU/ml (60 min) (Fig. 6Bi; Fig. S6A). Consistent with this trend, plaque plates showed visibly higher plaque density at longer centrifugation times, indicating improved

pelleting efficiency. Figure S7 also shows that extending centrifugation time after PEG/NaCl precipitation (15–60 min) significantly improved M13 recovery and reduced phage loss, with the highest recovery observed at 60 min. We also found that high-speed centrifugation alone can effectively recover M13 at very high starting titers ($\geq 1 \times 10^{13}$ PFU/ml). Extending centrifugation at 20000×*g* from 15 to 30 and 60 min significantly increased plaque density and phage titers (Fig. S8A and B), indicating that direct centrifugation can concentrate M13 without PEG/NaCl under high-titer conditions. We next fixed centrifugation at 60 min and varied PEG/NaCl precipitation duration independently (1 h, 4 h, and 16 h/overnight). Extended precipitation markedly improved phage recovery, increasing from approximately $\sim 1 \times 10^{13}$ PFU/ml (1 h) to $\sim 2 \times 10^{13}$ PFU/ml (4 h) and reaching $\sim 4 \times 10^{13}$ PFU/ml after overnight precipitation (Fig. 6Bi); Fig. S6B). These results indicate that longer PEG/NaCl incubation enhances precipitation completeness and phage capture, consistent with common phage purification workflows recommending ≥4 h or overnight precipitation to maximize recovery [39]. Therefore, these data demonstrate that both sufficient precipitation time and adequate centrifugation duration are critical determinants of PEG/NaCl-based M13 phage recovery. In contrast, optimized incubation time for PEG/NaCl precipitation followed by high-speed centrifugation has demonstrated superior recovery and preserved phage integrity, offering a faster, scalable, and reliable method for phage purification. Moreover, using this practice provided a higher M13 phage titer while ensuring both a high phage count and ultimately excellent phage quality. These findings indicate that PEG/NaCl precipitation followed by high-speed centrifugation is sufficient to achieve effective, filtration-free purification of M13 phage without increased bacterial carryover, consistent with established filamentous phage and phage display workflows [39]. This conclusion is further supported by bacterial contamination assays, which demonstrated a near-complete elimination of viable *E. coli* ER2738 following purification, with CFU/ml counts reduced by several orders of magnitude compared with unpurified samples (Fig. S9). Efficient purification of phage suspensions is crucial for downstream applications, particularly in phage display biopanning, where the removal of contaminants is essential [31]. Bacterial debris can interfere with phage binding and compromise the selection of high-affinity binders. Insufficient purification may lead to the unintended loss of valuable target-specific phages while retaining low-affinity clones, thereby impairing the identification of effective biorecognition elements (BREs) [31]. While filtration ensures high purity, it substantially reduces phage yield. PEG/NaCl precipitation, though widely used, also limits recovery. PEG/NaCl precipitation followed by high-speed centrifugation emerged as the most efficient strategy, balancing recovery and purity, both of which are essential for preserving the diversity and functionality of the M13 phage as well as the M13 phage display library in phage display biopanning.

Phage preservation strategies for long-term stability

Long-term glycerol storage is essential in phage display to maintain M13 phage viability and infectivity, ensuring that displayed peptides or proteins retain their functional binding properties in subsequent biopanning or assay rounds [39]. This is particularly crucial for preserving rare high-affinity binders enriched during later selection stages, protecting them from potential loss due to contamination, mutation, or technical errors [39]. Figure S10A demonstrates the long-term stability of M13 phage by comparing plaque titers at the time of initial storage and after one year in 15% glycerol at –80 °C. As shown in Fig. S10A, DAL assay plates at a 10^{-7} dilution exhibited comparable plaque densities before and after storage, while quantitative analysis in Fig. S10A confirmed that phage titers remained consistently around 1.8×10^{10} PFU/ml. Statistical analysis using an unpaired two-tailed Student's *t*-test revealed no significant difference ($P > .05$) between the initial and one-year titers, indicating that M13 viability

Table 2 Best-practice conditions for high-titre M13 amplification in *E. coli*.

Parameter	Recommended condition	Rationale/note
Host strain & baseline culture	*E. coli* K-12 ER2738 in LB at 37 °C, 250 rpm (early-log phase)	Matches host strain, temperature, and shaking conditions used throughout the study.
Host density at infection	Start infection in lag–early log phase (OD_{600} = 0.05–0.5)	Highest phage titers observed at low OD_{600}; yields decrease at $OD_{600} \geq 1.0$ despite continued bacterial growth.
Incubation time (amplification)	5 h at 37 °C, 250 rpm	Extension to 16 h (overnight) does not significantly increase phage yield at optimal host densities.
MOI/infection ratio (M13: *E. coli*)	2:1 (moderate MOI)	Produces the highest phage yield ($\sim 8 \times 10^{11}$ PFU/ml). Higher MOIs (≥10:1) reduce yield, likely due to combined effects of superinfection exclusion, reduced effective adsorption efficiency, and increased selection for phage-resistant mutants.
Aeration (shaking speed/vessel)	High aeration: 250 ml glass Erlenmeyer flask with 20 ml culture, 250 rpm	Enhanced oxygen transfer significantly increases phage yield compared to polypropylene tubes or lower shaking speeds.
Clarification/purification strategy	PEG/NaCl precipitation followed by high-speed centrifugation (20,000×*g*, ≥60 min, 4 °C)	Extended PEG/NaCl precipitation (4–16 h) combined with sufficient centrifugation time maximizes phage recovery; membrane filtration reduce apparent phage yield.
Long-term preservation ('phage banking')	15%–50% glycerol at –80 °C	Phage viability maintained for ≥1 year with no significant loss in titer across glycerol concentrations.

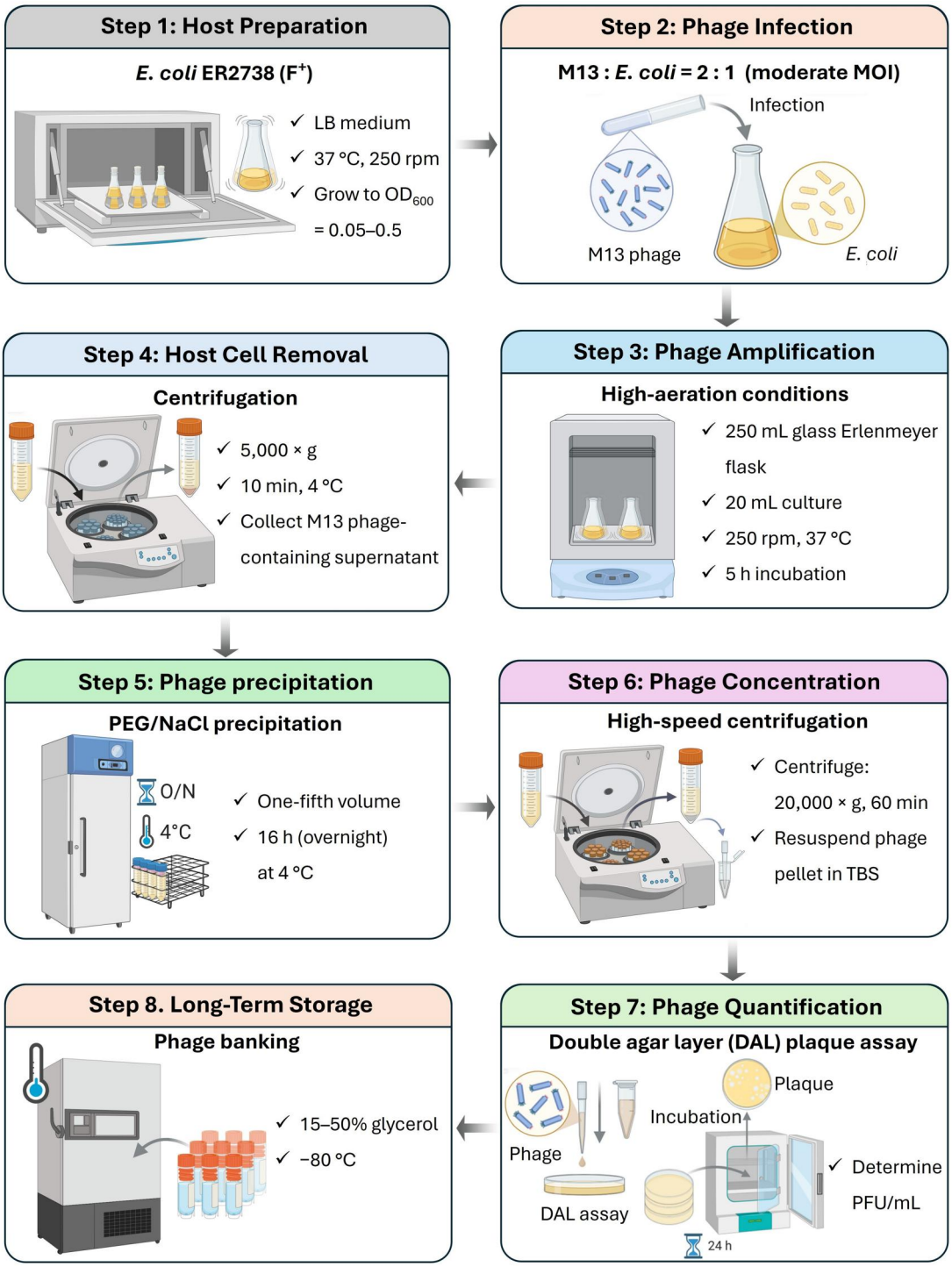

Figure 7 Optimized workflow for high-efficiency M13 phage propagation and purification. The flowchart summarizes the most efficient experimental pathway for M13 phage production identified in this study, including host preparation, phage infection at moderate multiplicity of infection, high-aeration amplification, cell removal, PEG/NaCl-based concentration, phage quantification, and long-term storage. Parameter choices reflect conditions yielding maximal phage titres while minimizing phage loss and bacterial contamination. This workflow is intended as a practical guideline for reproducible M13 phage propagation

was effectively preserved. In addition, Fig. S10B shows that M13 phage stocks prepared in 50% (v/v) glycerol (initial ~3.4×10^{11} PFU/ml) also retained comparable titers after one year at −80 °C, with no significant differences between the initial and one-year measurements ($P > .05$), confirming robust long-term viability across glycerol concentrations. The use of 15% to 50% glycerol as a cryoprotectant likely contributed to this stability by preventing ice crystal formation and preserving the structural integrity of the filamentous

phage capsid, which is essential for maintaining infectivity during freezing [97, 98]. This is especially critical for filamentous phages like M13, whose replication and infectivity are highly dependent on capsid structure [65, 99, 100]. These findings highlight the suitability of glycerol-based storage for phage display applications, where reproducibility and long-term access to enriched clones are critical. Furthermore, it ensures the availability of rare, high-affinity clones throughout extended research timelines, safeguarding the continuity and reliability of phage display studies.

To aid reproducibility, we summarize the optimized amplification and purification conditions for M13 phage in *E. coli* in Table 2.

Conclusion

In conclusion, this study identified and optimized critical parameters for enhancing the propagation and purification efficiency of M13 bacteriophage, significantly improving its application in phage display technologies. The research demonstrated that optimal phage amplification occurs under precise bacterial density conditions, controlled multiplicity of infection (MOI), and enhanced aeration, highlighting the detrimental impact of high MOI due to superinfection exclusion. This study determines that factors influencing the bacterial growth phase, specifically host density, multiplicity of infection, and aeration, collectively regulate the optimal conditions for maximal M13 phage yield. Additionally, optimal incubation time for PEG/NaCl precipitation followed by high-speed centrifugation was shown to substantially improve phage recovery compared to traditional filtration methods, addressing key purification challenges. To further support practical implementation, we have summarized the most efficient M13 propagation and purification workflow as a step-by-step flowchart at the end of the conclusion (Fig. 7). These findings offer a robust, scalable, and reproducible framework essential for generating high-quality M13 phage libraries, thus enabling more reliable and effective identification of biorecognition elements (BREs). Eventually, this work will contribute valuable insights that will significantly advance biosensor development and therapeutic applications, addressing existing gaps and paving the way for innovative diagnostic and industrial solutions.

Acknowledgements

M.M.H. gratefully acknowledges the Australian Government and RMIT University for supporting his PhD program through the RTP Stipend Scholarship (RSS). The authors thank the Ian Potter Foundation for establishing the Sir Ian Potter NanoBiosensing Facility at RMIT University, where the research was undertaken. Illustrations used in this manuscript were created with BioRender.com.

Author contributions

Md Monir Hossain (Conceptualization [equal], Data curation [lead], Formal analysis [equal], Investigation [equal], Methodology [equal], Validation [lead], Writing—original draft [lead], Writing—review & editing [equal]), Foong Yong (Conceptualization [equal], Investigation [equal], Supervision [equal], Visualization [equal], Writing—review & editing [equal]), Vipul Bansal (Conceptualization [equal], Formal analysis [equal], Funding acquisition [lead], Project administration [equal], Resources [lead], Supervision [equal], Visualization [equal], Writing—review & editing [equal]), and Ravi Shukla (Conceptualization [equal], Formal analysis [equal], Funding acquisition [equal], Investigation [equal], Project administration [equal], Resources [equal], Supervision [lead], Visualization [equal], Writing—review & editing [equal])

Supplementary material

Supplementary material is available at *Biology Methods and Protocols* online.

Conflicts of interest

The authors declare that the research was conducted in the absence of any commercial or financial relationships that could be construed as a potential conflict of interest.

Funding

V.B. acknowledges the Australian Research Council (ARC) for funding support through the Discovery scheme (DP230101650).

Data availability

All datasets generated for this study are included in the manuscript and the attached supporting information.

References

1. Analytica A. *Biosensors Market to Worth Over USD 75.84 Billion by 2033*. 2025. https://www.globenewswire.com/news-release/2025/04/16/3062540/0/en/Biosensors-Market-to-Worth-Over-USD-75-84-Billion-by-2033-Astute-Analytica.html (16 April 2025, date last accessed).
2. Badrick T. Evidence-based laboratory medicine. *Clin Biochem Rev* 2013;**34**:43–6.
3. Services, C. f. M. M. *FDA and CMS Statement: Americans Deserve Accurate and Reliable Diagnostic Tests, Wherever They Are Made*. 2024. https://www.cms.gov/newsroom/press-releases/fda-and-cms-statement-americans-deserve-accurate-and-reliable-diagnostic-tests-wherever-they-are (18 January 2024, date last accessed).
4. Baranwal A, Shukla R, Bansal V. Nanozyme-enhanced paper-based biosensor technologies. *TRAC Trends Anal Chem* 2024; **172**:117573.
5. Wu J, Liu H, Chen W *et al.* Device integration of electrochemical biosensors. *Nat Rev Bioeng* 2023;**1**:346–60.
6. Wang M, Yang Z, Liu X *et al.* Pathogen biosensors for food safety and public healthcare based on specific biological probes biopanned by phage display: a critical review. *Food Chem* 2025; **492**:145290.
7. Wang M, Pang S, Zhang H *et al.* Phage display based biosensing: recent advances and challenges. *TrAC Trends Anal Chem* 2024; **173**:117629.
8. Chambers JP, Arulanandam BP, Matta LL *et al.* Biosensor recognition elements. *Curr Issues Mol Biol* 2008;**10**:1–12.
9. Justino CI, Freitas AC, Pereira R *et al.* Recent developments in recognition elements for chemical sensors and biosensors. *TrAC Trends Anal Chem* 2015;**68**:2–17.
10. Naresh V, Lee N. A review on biosensors and recent development of nanostructured materials-enabled biosensors. *Sensors* 2021; **21**:1109.

11. Morales MA, Halpern JM. Guide to selecting a biorecognition element for biosensors. *Bioconjug Chem* 2018;**29**:3231–9.
12. Nguyen HH, Lee SH, Lee UJ *et al.* Immobilized enzymes in biosensor applications. *Materials* 2019;**12**:121.
13. Carpenter AC, Paulsen IT, Williams TC. Blueprints for biosensors: design, limitations, and applications. *Genes (Basel)* 2018;**9**:375.
14. Sande MG, Rodrigues JL, Ferreira D *et al.* Novel biorecognition elements against pathogens in the design of state-of-the-art diagnostics. *Biosensors (Basel)* 2021;**11**:418.
15. Xu P, Ghosh S, Gul AR *et al.* Screening of specific binding peptides using phage-display techniques and their biosensing applications. *TrAC Trends Anal Chem* 2021;**137**:116229.
16. Jaroszewicz W, Morcinek-Orłowska J, Pierzynowska K *et al.* Phage display and other peptide display technologies. *FEMS Microbiol Rev* 2022;**46**:fuab052.
17. Qi H, Wang F, Petrenko VA, Liu A. Peptide microarray with ligands at high density based on symmetrical carrier landscape phage for detection of cellulase. *Anal Chem* 2014;**86**:5844–50.
18. Ertürk G, Lood R. Bacteriophages as biorecognition elements in capacitive biosensors: phage and host bacteria detection. *Sensors Actuators B Chem* 2018;**258**:535–43.
19. Janczuk M, Niedziółka-Jönsson J, Szot-Karpińska K. Bacteriophages in electrochemistry: a review. *J Electroanal Chem* 2016;**779**:207–19.
20. Pires DP, Cleto S, Sillankorva S *et al.* Genetically engineered phages: a review of advances over the last decade. *Microbiol Mol Biol Rev* 2016;**80**:523–43.
21. Han L, Xia H, Yin L *et al.* Selected landscape phage probe as selective recognition interface for sensitive total prostate-specific antigen immunosensor. *Biosens Bioelectron* 2018;**106**:1–6.
22. Ahovan Z, Hashemi A, De Plano L *et al.* Bacteriophage based biosensors: trends, outcomes and challenges. *Nanomaterials* 2020;**10** (3): 501.
23. Petrenko VA. Landscape phage: evolution from phage display to nanobiotechnology. *Viruses* 2018;**10**:311.
24. Peltomaa R, Benito-Peña E, Barderas R, Moreno-Bondi MC. Phage display in the quest for new selective recognition elements for biosensors. *Acs Omega* 2019;**4**:11569–80.
25. Allen GL, Grahn AK, Kourentzi K *et al.* Expanding the chemical diversity of M13 bacteriophage. *Front Microbiol* 2022;**13**:961093.
26. Wang R, Li H-D, Cao Y *et al.* M13 phage: a versatile building block for a highly specific analysis platform. *Anal Bioanal Chem* 2023; **415**:3927–44.
27. Chang C, Guo W, Yu X *et al.* Engineered M13 phage as a novel therapeutic bionanomaterial for clinical applications: from tissue regeneration to cancer therapy. *Mater Today Bio* 2023;**20**:100612.
28. Pande J, Szewczyk MM, Grover AK. Phage display: concept, innovations, applications and future. *Biotechnol Adv* 2010;**28**:849–58.
29. Panagides N, Zacchi LF, De Souza MJ *et al.* Evaluation of phage display biopanning strategies for the selection of anti-cell surface receptor antibodies. *Int J Mol Sci* 2022;**23**:8470.
30. Lim CC, Woo PC, Lim TS. Development of a phage display panning strategy utilizing crude antigens: isolation of MERS-CoV nucleoprotein human antibodies. *Sci Rep* 2019;**9**:6088.
31. Branston SD. An investigation of the properties of bacteriophage M13 and the implications for its large-scale bioprocessing. UCL (University College London), 2010.
32. Caffin C, Milhamont L, Duriez E *et al.* Optimization of bacteriophage propagation in high-yield continuous culture (cellstat) meeting the constraints of industrial manufacturing processes. *J Biosci Bioeng* 2024;**138**:507–14.
33. Harb L, Chamakura K, Khara P *et al.* ssRNA phage penetration triggers detachment of the F-pilus. *Proc Natl Acad Sci USA* 2020; **117**:25751–8.
34. Labrie SJ, Samson JE, Moineau S. Bacteriophage resistance mechanisms. *Nat Rev Microbiol* 2010;**8**:317–27.
35. Harada LK, Silva EC, Campos WF *et al.* Biotechnological applications of bacteriophages: state of the art. *Microbiol Res* 2018; **212–213**:38–58.
36. Tay MY, Lee CC, Vasudevan SG, Moreland NJ. Identification of dengue-specific human antibody fragments using phage display. *Methods Mol Biol* 2014;**1138**:161–73.
37. Ciric M, Ng F, Rakonjac J, Gagic D. Metasecretome phage display. In: Hust, M., Lim, T. (eds) *Phage Display: Methods and Protocols*, Springer, 2017, 519–34. Humana Press, New York, NY.
38. Biolabs NE. *Ph.D.™ Phage Display Peptide Library Kits v2*. 2025. https://www.neb.com/en-au/products/e8210-phd-12-phage-display-peptide-library-kit-v2 (accessed 2026, date last accessed).
39. Barbas CF. Phage display: a laboratory manual. 2001. Cold Spring Harbor Laboratory Press, Cold Spring Harbor, NY, USA.
40. Sambrook J, David W. *Molecular Cloning: A Laboratory Manual*, 3rd edn. Cold New York; Spring Harbor Laboratory Press; 2001.
41. Xu H, Li L, Deng B *et al.* Construction of a T7 phage display nanobody library for bio-panning and identification of chicken dendritic cell-specific binding nanobodies. *Sci Rep* 2022;**12**:12122.
42. Tanaka AS, Silva MM, Torquato RJ *et al.* Functional phage display of leech-derived tryptase inhibitor (LDTI): construction of a library and selection of thrombin inhibitors. *FEBS Lett* 1999; **458**:11–6.
43. Kulseth MA, Fagerlund A, Myrset AH. Affinity selection using filamentous phage display. In: Nixon, A. (eds) *Therapeutic Peptides: Methods and Protocols*, Springer, 2013; 67–80. Humana Press, Totowa, NJ.
44. Zade HM, Keshavarz R, Shekarabi HSZ, Bakhshinejad B. Biased selection of propagation-related TUPs from phage display peptide libraries. *Amino Acids* 2017;**49**:1293–308.
45. Abedon ST. Phage therapy dosing: the problem (s) with multiplicity of infection (MOI). *Bacteriophage* 2016;**6**:e1220348.
46. Caro LG, Schnös M. The attachment of the male-specific bacteriophage F1 to sensitive strains of *Escherichia coli*. *Proc Natl Acad Sci USA* 1966;**56**:126–32.
47. Fareed G, Ippen KA, Valentine RC. Active fragments of a filamentous bacteriophage. *Biochem Biophys Res Commun* 1966; **25**:275–84.
48. Nguyen TVP, Wu Y, Yao T *et al.* Coinfecting phages impede each other's entry into the cell. *Curr Biol* 2024;**34**:2841–53. e18. e2818.
49. Necel A, Bloch S, Nejman-Faleńczyk B *et al.* A validation system for selection of bacteriophages against Shiga toxin-producing *Escherichia coli* contamination. *Toxins (Basel)* 2021;**13**:644.
50. Mancuso F. *Bioprocessing of Bacteriophages and Bacteriocins: Continuous Culture and Downstream Purification*. (Doctoral dissertation), Loughborough University, Loughborough, UK, 2019.
51. Bourdin G, Schmitt B, Marvin Guy L *et al.* Amplification and purification of T4-like *Escherichia coli* phages for phage therapy: from laboratory to pilot scale. *Appl Environ Microbiol* 2014;**80**:1469–76.
52. Mira P, Yeh P, Hall BG. Estimating microbial population data from optical density. *PLoS One* 2022;**17**:e0276040.
53. Liu Y, Su A, Tian R *et al.* Developing rapid growing Bacillus subtilis for improved biochemical and recombinant protein production. *Metab Eng Commun* 2020;**11**:e00141.

54. Heusser K, Heusser R, Jordan J *et al.* Baroreflex curve fitting using a WYSIWYG boltzmann sigmoidal equation. *Front Neurosci* 2021; **15**:697582.
55. Hossain MM, Polash SA, Takikawa M *et al.* Investigation of the antibacterial activity and in vivo cytotoxicity of biogenic silver nanoparticles as potent therapeutics. *Front Bioeng Biotechnol* 2019;**7**:239.
56. Niloy MS, Hossain MM, Takikawa M *et al.* Synthesis of biogenic silver nanoparticles using Caesalpinia digyna and investigation of their antimicrobial activity and in vivo biocompatibility. *ACS Appl Bio Mater* 2020;**3**:7722–33.
57. Mahmud KM, Hossain MM, Polash SA *et al.* Investigation of antimicrobial activity and biocompatibility of biogenic silver nanoparticles synthesized using syzigyum cymosum extract. *ACS Omega* 2022;**7**:27216–29.
58. Fang Q, Feng Y, McNally A, Zong Z. Characterization of phage resistance and phages capable of intestinal decolonization of carbapenem-resistant Klebsiella pneumoniae in mice. *Commun Biol* 2022;**5**:48.
59. Montso PK, Mlambo V, Ateba CN. Characterization of lytic bacteriophages infecting multidrug-resistant shiga toxigenic atypical *Escherichia coli* O177 strains isolated from cattle feces. *Front Public Health* 2019;**7**:355.
60. Smith GP. Filamentous fusion phage: novel expression vectors that display cloned antigens on the virion surface. *Science* 1985; **228**:1315–7.
61. Sidhu SS. Engineering M13 for phage display. *Biomol Eng* 2001; **18**:57–63.
62. Warner CM, Barker N, Lee S-W, Perkins EJ. M13 bacteriophage production for large-scale applications. *Bioprocess Biosyst Eng* 2014;**37**:2067–72.
63. Krishnan R, Tsubery H, Proschitsky MY *et al.* A bacteriophage capsid protein provides a general amyloid interaction motif (GAIM) that binds and remodels misfolded protein assemblies. *J Mol Biol* 2014;**426**:2500–19.
64. Choi YK, Han SM, Lee SM *et al.* Investigation of the relation between temperature and M13 phage production via ATP expenditure. *Processes* 2022;**10**:962.
65. Smeal SW, Schmitt MA, Pereira RR *et al.* Simulation of the M13 life cycle I: assembly of a genetically-structured deterministic chemical kinetic simulation. *Virology* 2017;**500**:259–74.
66. Sauvageau D, Cooper DG. Two-stage, self-cycling process for the production of bacteriophages. *Microb Cell Fact* 2010;**9**:81–10.
67. Nabergoj D, Modic P, Podgornik A. Effect of bacterial growth rate on bacteriophage population growth rate. *MicrobiologyOpen* 2018;**7**:e00558.
68. Silva J, Dias R, Junior JI *et al.* A rapid method for performing a multivariate optimization of phage production using the RCCD approach. *Pathogens* 2021;**10**:1100.
69. Kim SG, Kwon J, Giri SS *et al.* Strategy for mass production of lytic Staphylococcus aureus bacteriophage pSa-3: contribution of multiplicity of infection and response surface methodology. *Microb Cell Fact* 2021;**20**:56–12.
70. Hodges FE, Sicheritz-Pontén T, Clokie MR. The effect of oxygen availability on bacteriophage infection: a review. *Phage (New Rochelle)* 2021;**2**:16–25.
71. Ács N, Gambino M, Brøndsted L. Bacteriophage enumeration and detection methods. *Front Microbiol* 2020;**11**:594868.
72. Wan Z, Goddard NL. Competition between conjugation and M13 phage infection in *Escherichia coli* in the absence of selection pressure: a kinetic study. *G3 (Bethesda)* 2012;**2**:1137–44.
73. Mancuso F, Shi J, Malik DJ. High throughput manufacturing of bacteriophages using continuous stirred tank bioreactors connected in series to ensure optimum host bacteria physiology for phage production. *Viruses* 2018;**10**:537.
74. Hernández S, Vives MJ. Phages in anaerobic systems. *Viruses* 2020;**12**:1091.
75. Hadas H, Einav M, Fishov I, Zaritsky A. Bacteriophage T4 development depends on the physiology of its host *Escherichia coli*. *Microbiology (Reading)* 1997;**143**:179–85.
76. Hernández Villamizar S, Chica Cárdenas LA, Morales Mancera LT, Vives Florez MJ. Anaerobiosis, a neglected factor in phage-bacteria interactions. *Appl Environ Microbiol* 2023;**89**:e01491-01423.
77. Kourilsky P. Lysogenization by bacteriophage lambda: i. multiple infection and the lysogenic response. *Molec Gen Genet* 1973; **122**:183–95.
78. Geng Y, Nguyen TVP, Homaee E, Golding I. Using population dynamics to count bacteriophages and their lysogens. bioRxiv, 2023, preprint: not peer reviewed.
79. Shotland Y, Shifrin A, Ziv T *et al.* Proteolysis of bacteriophage λ CII by *Escherichia coli* FtsH (HflB). *J Bacteriol* 2000;**182**:3111–6.
80. Kobiler O, Rokney A, Oppenheim AB. Phage lambda CIII: a protease inhibitor regulating the lysis-lysogeny decision. *PLoS One* 2007;**2**:e363.
81. Tumban E. *Bacteriophages*; Springer, 2024. Humana Press, New York Plaza, New York, NY 10004, U.S.A
82. Stocker G, Dumoulin D, Vandevyver C *et al.* Screening of a human antibody phage display library against a peptide antigen using stimuli-responsive bioconjugates. *Biotechnol Prog* 2008;**24**:1314–24.
83. Bucher MJ, Czyż DM. Phage against the machine: the SIE-ence of superinfection exclusion. *Viruses* 2024;**16**:1348.
84. Pathania A, Hopper C, Pandi A *et al.* A synthetic communication system uncovers self-jamming of bacteriophage transmission. bioRxiv, 2022, preprint: not peer reviewed. https://doi.org/10.1101/2022.05.11.491355
85. Boeke JD, Model P, Zinder ND. Effects of bacteriophage f1 gene III protein on the host cell membrane. *Mol Gen Genet* 1982; **186**:185–92.
86. Richter Ł, Księżarczyk K, Paszkowska K *et al.* Adsorption of bacteriophages on polypropylene labware affects the reproducibility of phage research. *Sci Rep* 2021;**11**:7387.
87. Grieco S-HH, Lee S, Dunbar WS *et al.* Maximizing filamentous phage yield during computer-controlled fermentation. *Bioprocess Biosyst Eng* 2009;**32**:773–9.
88. Malik DJ, Sokolov IJ, Vinner GK *et al.* Formulation, stabilisation and encapsulation of bacteriophage for phage therapy. *Adv Colloid Interface Sci* 2017;**249**:100–33.
89. Castillo T, Heinzle E, Peifer S *et al.* Oxygen supply strongly influences metabolic fluxes, the production of poly (3-hydroxybutyrate) and alginate, and the degree of acetylation of alginate in *Azotobacter vinelandii*. *Process Biochem* 2013;**48**:995–1003.
90. Izadi P, Izadi P, Eldyasti A. Evaluation of PAO adaptability to oxygen concentration change: development of stable EBPR under stepwise low-aeration adaptation. *Chemosphere* 2022;**286**:131778.
91. Stopar D, Jansen KA, Páli T *et al.* Membrane location of spin-labeled M13 major coat protein mutants determined by paramagnetic relaxation agents. *Biochemistry* 1997;**36**:8261–8.
92. Li M, Wen K, Li Y, Zhu L. Impact of oxygen availability on microbially induced calcite precipitation (MICP) treatment. *Geomicrobiol J* 2018;**35**:15–22.
93. Chilmawati D, Hutabarat J, Anggoro S, Suminto S. Effects of Aeration Flow Rate in the Culture Medium on the Growth

Performance and Egg Production of Copepod Oithona similis Fed with Fermented Organic Diet. *E3s Web Conf* 2020; **147**:01006.
94. Griffiths MH, Andrew PW, Ball PR, Hall GM. Rapid methods for testing the efficacy of sterilization-grade filter membranes. *Appl Environ Microbiol* 2000;**66**:3432–7.
95. Große-Leppkes DJ. *How to Choose the Right Membrane for Your Syringe Filter*. KNAUER, 2024. https://store.knauer.net/blog/knauer-blog-7/how-to-choose-the-right-membrane-for-your-syringe-filter-30 (30 September 2025, date last accessed).
96. Corning. *Corning® Filtration Guide*. Corning Incorporated Life Sciences, 2024. https://www.corning.com/catalog/cls/documents/selection-guides/t_filterselectionguide.pdf (accessed 2026, date last accessed).
97. Fortier L-C, Moineau S. Phage production and maintenance of stocks, including expected stock lifetimes. *Methods Mol Biol* 2009; **501**:203–19.
98. Pegg DE. Principles of cryopreservation. *Methods Mol Biol* 2015; **1257**:3–19.
99. Rakonjac J, Bennett NJ, Spagnuolo J *et al.* Filamentous bacteriophage: biology, phage display and nanotechnology applications. *Curr Issues Mol Biol* 2011;**13**:51–76.
100. Hay ID, Lithgow T. Filamentous phages: masters of a microbial sharing economy. *EMBO Rep* 2019;**20**:e47427.

Biology Methods and Protocols, 2026, 11, 1–18
https://doi.org/10.1093/biomethods/bpag011
Methods Article